Understanding ecosystem gross primary productivity, evapotranspiration, and water use efficiency of maize using ISBA-A-g_s land surface model over temperate and tropical semi-arid climates

Syam Chintala[1*], Lionel Jarlan[2], Vincent Rivalland[2], Aaron Boone[3], Oluwakemi Dare-Idowu[4,5], Valerie Le Dantec[2], Gilles Boulet[2,6], BVN P. Kambhammettu[1] and Aurore Brut[2]

[1]Department of Civil Engineering, Indian Institute of Technology Hyderabad, Sangareddy, Telangana, India.

[2]CESBIO, Universite de Toulouse, CNES/CNRS/INRAE/IRD, Toulouse, France.

[3]Centre National de Recherche's Meteorological (CNRM), Meteo-France/CNRS, Toulouse, France.

[4]Agricome Project Solutions Limited, Abuja, Nigeria.

[5]Lead City University, Ibadan, Nigeria.

[6]Indo-French Cell for Water Sciences, ICWaR, Indian Institute of Science, Bangalore, India.

*Corresponding author: Syam Chintala, E-mail: ce22resch11012@iith.ac.in, Tel: +91 7997014429

Abstract

Water use efficiency (WUE) links carbon assimilation and water loss and is an important indicator of ecosystem functioning under changing hydroclimatic conditions. Process-based land surface models (LSMs) provide a framework for simulating carbon-water interactions, but their ability to reproduce ecosystem-scale WUE across contrasting climates remains insufficiently evaluated. This study assesses the performance of the ISBA-A-g_s land surface model, implemented within the SURFEX platform, in simulating gross primary productivity

(GPP), evapotranspiration (ET), and WUE (GPP/ET) for maize under temperate conditions in France (FR-Lam) and tropical semi-arid conditions in India (Ind-IITH). The model was driven by site-specific meteorological and vegetation data across six growing seasons at FR-Lam under sprinkler irrigation and two growing seasons at Ind-IITH, representing monsoon and winter crops under alternate furrow irrigation (AFI). Model calibration indicated contrasting controls on carbon and water exchanges between the two sites. At FR-Lam, relatively higher cuticular conductance and stronger atmospheric control on stomatal behaviour were identified, whereas at Ind-IITH, mesophyll conductance and soil moisture stress thresholds were important calibration parameters. At FR-Lam, the model simulated mean seasonal cumulative GPP, ET, and WUE of 1039 ± 20 gC m^{-2}, 610 ± 31 kg H_2O m^{-2}, and 1.70 ± 0.10 gC kg^{-1} H_2O, respectively, compared with measured values of 1026 ± 30 gC m^{-2}, 562 ± 42 kg H_2O m^{-2}, and 1.82 ± 0.11 gC kg^{-1} H_2O. At Ind-IITH, simulated values were 766 ± 15 gC m^{-2}, 567 ± 30 kg H_2O m^{-2}, and 1.35 ± 0.11 gC kg^{-1} H_2O, compared with measured values of 793 ± 11 gC m^{-2}, 522 ± 20 kg H_2O m^{-2}, and 1.51 ± 0.12 gC kg^{-1} H_2O. Diagnostic analysis based on underlying water use efficiency (uWUE) further indicated that the model reproduced the relationship between carbon assimilation and transpiration-driven water loss. Overall, ISBA-A-g_s captured the seasonal dynamics of maize carbon and water exchanges across the two contrasting climates, although differences between simulated and measured ET and WUE remained. The results highlight the potential of process-based modelling to assess carbon-water coupling across diverse hydroclimatic conditions and provide insights into the physiological controls governing crop water use.

Keywords: Ecosystem modelling, Gross primary productivity, Evapotranspiration, Water use efficiency, Maize, Climate.

Research Highlights:

1. Multi-energy balance ISBA-A-g_s was applied to simulate maize WUE across temperate and tropical semi-arid climates.
2. Parameter calibration improved GPP simulations more substantially than ET.
3. The model reproduces irrigation-driven divergence in tropical semi-arid conditions, reflecting robust soil moisture stress and canopy resistance parameterization.
4. ISBA-A-g_s successfully reproduces the realistic coupling between photosynthesis and transpiration, as revealed by the underlying water use efficiency (uWUE) framework.

1.0 Introduction

Water use efficiency (WUE) links carbon assimilation and water loss and is widely used to assess terrestrial ecosystem functioning and carbon-water interactions (Chen et al., 2022; Ito and Inatomi, 2012; Yu et al., 2008). At the ecosystem scale, WUE is commonly defined as the ratio of gross primary productivity (GPP) to evapotranspiration (ET), providing an integrated measure of carbon uptake relative to water loss (Beer et al., 2009; Vadez et al., 2023). Eddy covariance (EC) measurements are widely used to quantify carbon and water exchanges across ecosystems through international networks such as FLUXNET, NEON, ICOS, and AmeriFlux (Aubinet et al., 1999; Baldocchi, 2014; Baldocchi et al., 2001; Pastorello et al., 2020; Reichstein et al., 2005). However, EC measurements are often challenged by their spatial representativeness, high installation and maintenance costs, and sensitivity to surface heterogeneity (Hoover et al., 2023). Land surface models (LSMs) offer a complementary tool by representing the coupled physical, hydrological, and physiological processes governing exchanges between vegetation, soil, and the atmosphere. As a class of soil vegetation atmosphere transfer (SVAT) models, LSMs simulate key processes such as photosynthesis, evapotranspiration, canopy conductance, soil moisture dynamics, and surface energy balance

(Calvet, 2000; Knorr and Heimann, 1995; Noilhan and Planton, 1989). They therefore provide a process-based framework for investigating carbon-water coupling across different environmental conditions.

The Interactions between Soil, Biosphere, and Atmosphere (ISBA) scheme, originally developed by Noilhan & Planton (1989), is implemented within the SURFEX modelling platform maintained by Meteo-France (Masson et al., 2013). The ISBA family includes different configurations to represent land surface exchanges. The classical formulation uses a composite soil-vegetation surface temperature, whereas the Multi-Energy Balance (MEB) configuration (ISBA-MEB) explicitly separates soil and vegetation energy budgets, allowing a more detailed representation of heterogeneous surface exchanges (Boone et al., 2017). ISBA-MEB has been evaluated across grasslands and croplands in France (Boone et al., 2017; Dare-Idowu et al., 2021), irrigated and rainfed grasslands in Spain (Martí et al., 2026) and olive orchards and wheat fields in Morocco (Aouade et al., 2020). However, the performance and transferability of ISBA-based approaches for simulating carbon-water exchanges remain insufficiently assessed across contrasting hydroclimatic conditions, particularly in tropical semi-arid regions. In these environments, high atmospheric demand, strong solar radiation, seasonal rainfall, and irrigation-driven soil moisture variability can strongly influence stomatal regulation, photosynthesis, and evapotranspiration.

Maize (*Zea mays L.*) is a major cereal crop cultivated across a wide range of climatic conditions and used for food, feed, and bioenergy (Erenstein et al., 2022; Tanumihardjo et al., 2020). Its carbon assimilation, water use, and productivity are strongly influenced by climate, soil moisture availability, and irrigation management. These controls differ substantially between temperate and tropical semi-arid agroecosystems. In temperate regions such as France, maize is generally grown during the summer under relatively consistent seasonal conditions. In tropical semi-arid regions of India, maize may be cultivated during both the monsoon and

winter seasons, with rainfed and irrigated production systems experiencing high atmospheric demand and pronounced variations in water availability. These contrasting conditions provide an opportunity to examine how climate and water management influence carbon-water coupling. Despite the extensive cultivation of maize in both regions, long-term field observations of ecosystem carbon and water fluxes remain limited, particularly in semi-arid agricultural systems (Scott et al., 2023). Evaluating LSM performance across these contrasting environments is therefore important for identifying the strengths and limitations of model parameterizations and assessing their transferability under different climatic and water management conditions.

France and India provide contrasting examples of maize production and irrigation practices. In France, maize covers approximately 1.52 million hectares and accounts for nearly 17% of cereal production, with irrigation representing a substantial share of agricultural water use (Battude et al., 2017). In India, maize is cultivated over more than 9 million hectares and contributes approximately 10% of global production. Reported maize WUE values are around 3.5 gC Kg^{-1} H_2O in France and 1.83 gC Kg^{-1} H_2O in India, compared with a global average of approximately 4-5 gC Kg^{-1} H_2O (FAO, 2017; Sharma et al., 2018). Irrigation practices also differ between the two regions. French maize is commonly irrigated using sprinkler systems, whereas furrow irrigation is widely practised in India. Conventional furrow irrigation can lead to uneven soil wetting, increased soil evaporation, and deep percolation, potentially reducing WUE. Alternative strategies, including regulated deficit irrigation, conservation tillage, and alternate furrow irrigation (AFI), have been investigated to improve water productivity while maintaining crop yields (Al-Kayssi, 2023; Li et al., 2007; Yang et al., 2012). AFI alternates irrigation between adjacent furrows, modifying soil moisture distribution and root water uptake while potentially reducing irrigation inputs without substantial yield penalties (Chintala and Kambhammettu, 2026; Kang et al., 1998, 2001). These changes can also affect stomatal

126 regulation, transpiration, and carbon assimilation. However, their combined effects on
127 ecosystem-scale carbon and water exchanges remain insufficiently quantified, particularly
128 under semi-arid conditions.

129 Understanding these responses requires a model that represents the interactions among soil
130 moisture, atmospheric demand, stomatal conductance, photosynthesis, and evapotranspiration.
131 The ISBA-A-g_s model incorporates a photosynthesis-based stomatal conductance scheme,
132 allowing carbon assimilation and transpiration to respond dynamically to environmental
133 conditions (Calvet, 2000). Nevertheless, stomatal regulation involves complex physiological
134 responses to radiation, vapour pressure deficit (VPD), and soil water availability that cannot be
135 fully described by physical conservation laws alone (Buckley, 2017; Cowan and GD, 1977;
136 Medlyn et al., 2011). Evaluating the model's ability to reproduce these responses is therefore
137 essential for understanding its representation of carbon-water coupling. In addition to
138 conventional WUE, underlying water use efficiency (uWUE) provides a complementary
139 diagnostic by normalizing GPP with the square root of VPD. This formulation accounts for the
140 theoretically predicted inverse square-root dependence of stomatal conductance on VPD under
141 optimal stomatal regulation (Zhou et al., 2014). By reducing the first-order influence of
142 atmospheric demand, uWUE can help assess the consistency of modelled carbon-water
143 relationships and distinguish physiological responses from variations driven primarily by
144 atmospheric conditions.

145 A systematic survey of the Scopus database covering 2004-2024, using the keywords
146 "*ecosystem modelling"*, *"modelling GPP and ET"*, *"modelling WUE"*, and *"land surface*
147 *modelling on WUE"* identified a limited number of studies addressing the simultaneous
148 modelling of carbon and water exchanges. The survey returned only four studies on GPP
149 modelling and ten on ET modelling, with no identified study examining ecosystem-scale WUE
150 using a locally calibrated LSM across contrasting climatic regimes. The modelling of WUE

under contrasting irrigation treatments, particularly in semi-arid Indian agroecosystems, also remains poorly investigated. Addressing these gaps is important for evaluating the capacity of process-based models to represent carbon-water interactions under different climatic conditions and irrigation strategies. This study aims to evaluate and apply the ISBA-A-g_s land surface model to investigate maize carbon-water coupling across temperate conditions in France and tropical semi-arid conditions in India. Specifically, the objectives are to: (i) characterize the seasonal dynamics of GPP, ET, and WUE in maize under contrasting climatic conditions and irrigation treatments; (ii) calibrate and validate ISBA-A-g_s using site-specific parameterizations; (iii) simulate GPP, ET, and WUE using the calibrated model across the study sites; and (iv) diagnose the model's ability to reproduce the eco-physiological mechanisms governing carbon-water coupling, including the responses to atmospheric demand. Using comprehensive field measurements of carbon and water fluxes, this study provides a cross-climatic assessment of model performance and explores the influence of irrigation management on maize carbon assimilation and water use.

2.0 Material and Methods

2.1 Experimental sites description

2.1.1 Lamasquere, France (FR-Lam)

The Lamasquere experimental site (FR-Lam; 43°50′05″ N, 1°24′19″ E; 180 m above mean sea level) covers a flat area of 24 ha, surrounded on its west and south sides by forest and is located about 25 km southwest of Toulouse, France (Figure 1). According to the Köppen-Geiger climate classification, FR-Lam is categorized as a temperate oceanic climate (Cfb) (Kottek et al., 2006). The regional wind regime is dominated by westerly and south-easterly winds, with an average wind speed of 1.8 m s^{-1}. The site follows a regular 2-year crop rotation with wheat in the first year and intermediate cover followed by maize (summer crop) in the

second year. Therefore, only years cultivated with maize were selected for this study (2006, 2008, 2010, 2012, 2014, and 2015). Summer maize (silage) is generally sown between April and May, irrigated during the mid-season, and harvested from late August to early September. Pivot irrigation was applied during 2008 and 2010, whereas sprinkler irrigation was adopted in the remaining years. Details of the crop cycles and associated biophysical variables for the selected seasons are provided in Table 1.

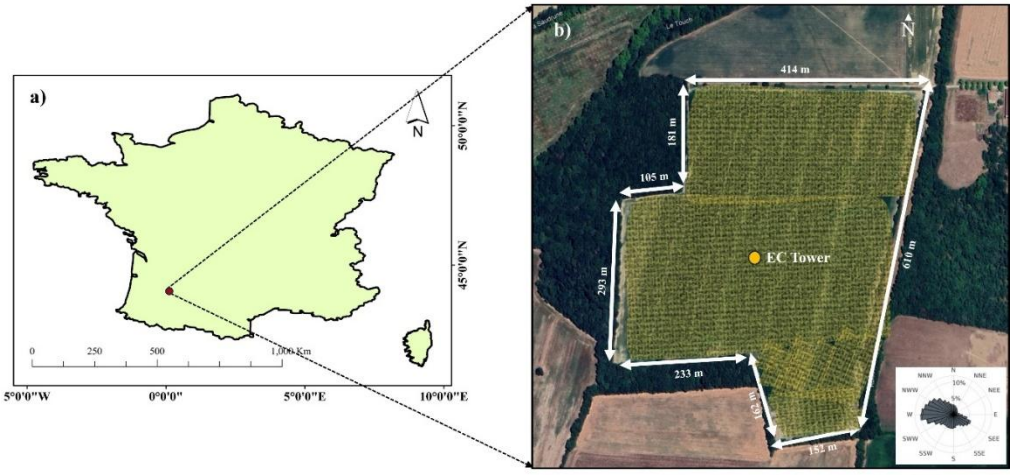


Figure 1. Overview of the FR-Lam experimental site: **(a)** Location of the study site; **(b)** Field extent and position of the EC tower within the site (Inset: observed wind rose diagram). Map source: The base map was designed and developed by Esri | Powered by Esri.

Table 1. Maize crop cycles with total rainfall and irrigation, sowing and harvest dates, crop length and maximum leaf area index (LAI) at FR-Lam experimental site.

Crop season	Rain [mm]	Irrigation [mm]	Total water [mm]	Sowing Date [DD/MM/YYYY]	Harvest Date [DD/MM/YYYY]	Crop length [Days]	Max LAI [m^2 m^{-2}]	Atmospheric evaporative demand ET_o [mm]
2006	265.5	45.25	310.75	01/05/2006	31/08/2006	123	3.1	403
2008	269.67	27.30	296.97	20/05/2008	11/09/2008	124	3.8	363
2010	196.61	106.10	302.61	21/04/2010	20/09/2010	138	4.0	432

2012	410.07	148.70	558.07	27/04/2012	23/08/2012	122	5.8	374
2014	331.05	167.70	498.05	14/05/2014	22/09/2014	131	5.2	388
2015	354.41	120.00	474.41	05/05/2015	08/09/2015	128	6.6	435

Monthly variations in major meteorological variables in Figure 2 shows that, 2008 received the lowest rainfall (270 mm), whereas 2012 recorded the highest (410 mm), corresponding to distinctly dry and wet years, respectively. Supplemental irrigation was primarily required during July and August (393 mm), coinciding with the peak vegetative growth stage (dough) for all the years. The balance between total available water (precipitation + irrigation) and atmospheric evaporative demand (ET_o) further highlighted interannual contrasts, with positive (+184 mm) and negative (-66 mm) water surpluses observed during 2012 and 2008, respectively. Seasonal mean air temperature ranged from 17 ± 1.60°C in 2012 to 19.50 ± 1.20°C in 2008, consistent with rainfall-driven wet and dry classifications. Similarly, mean VPD varied from 0.67 ± 0.10 kPa in 2012 to 0.78 ± 0.10 kPa in 2008, indicating greater atmospheric water demand in dry seasons. LAI displayed strong seasonal variability, with lower values observed in 2006 (3.1 m^2 m^{-2}), 2008 (3.9 m^2 m^{-2}), and 2010 (4 m^2 m^{-2}) compared to later years (2012: 5.9 m^2 m^{-2}; 2014: 5.2 m^2 m^{-2}; 2015: 6.6 m^2 m^{-2}). Overall, the FR-Lam site exhibited pronounced seasonal and interannual variability, with relatively drier conditions during the early seasons (2006, 2008, and 2010) and wetter conditions in later years (2012, 2014, and 2015). In addition to climatic variability, a change in maize cultivar between 2014 and 2015 contributed to improved canopy development and higher yield, indicating that both environmental conditions and management practices influenced crop performance.

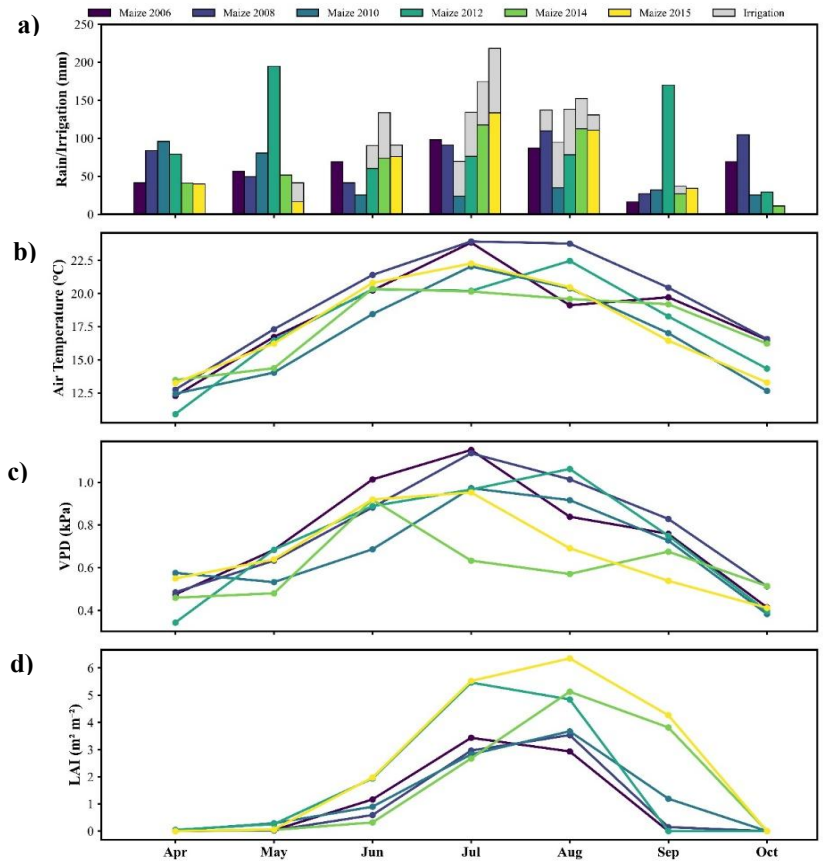


Figure 2. Monthly variations in environmental variables, including rainfall/Irrigation (cumulative values) **(a)**; Air temperature **(b)**; Vapor pressure deficit **(c)**; and Leaf area index **(d)** observed at FR-Lam experimental site during maize growing seasons.

2.1.2 Hyderabad, India (Ind-IITH)

Field experiments were conducted at the Ind-IITH site (17°35′48.44″ N, 78°07′05.78″ E; 549 m above mean sea level) in two adjacent agricultural fields located nearly 2 km from the Indian Institute of Technology Hyderabad (IITH), Telangana, India (Figure 3). Each field measures 100 m in length × 62 m in width, covering an area of about 0.62 ha. According to the Köppen-Geiger climate classification, the region falls under a tropical savannah climate (Aw), characterized by long dry periods and a short, intense wet season (Kottek et al., 2006). The regional wind regime is dominated by strong easterly winds, with an average wind speed of 1.05 m s^{-1}. Cropping patterns in the region are largely confined to two seasons, namely: the

monsoon (kharif) and winter (rabi). During the monsoon season, maize is typically sown in mid-June and harvested by early October, whereas winter maize is sown in early December and harvested by early April. Two irrigation treatments, continuous furrow irrigation (CFI) and alternate furrow irrigation (AFI), were implemented, with irrigation water applied uniformly to all furrows under CFI and alternated between furrows based on the prevailing soil moisture conditions under AFI. Details of the crop cycles and associated biophysical variables for the selected seasons are summarized in Table 2.

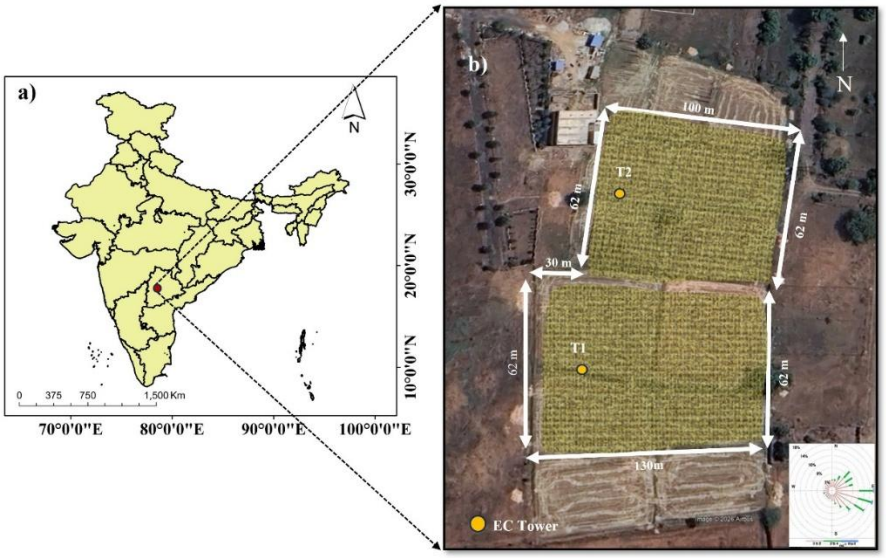


Figure 3. Overview of the Ind-IITH experimental site: **(a)** Location of the study site; **(b)** Field extent and position of the EC towers within the site (Inset: Observed Windrose diagram). Map source: The base map was designed and developed by Esri | Powered by Esri.

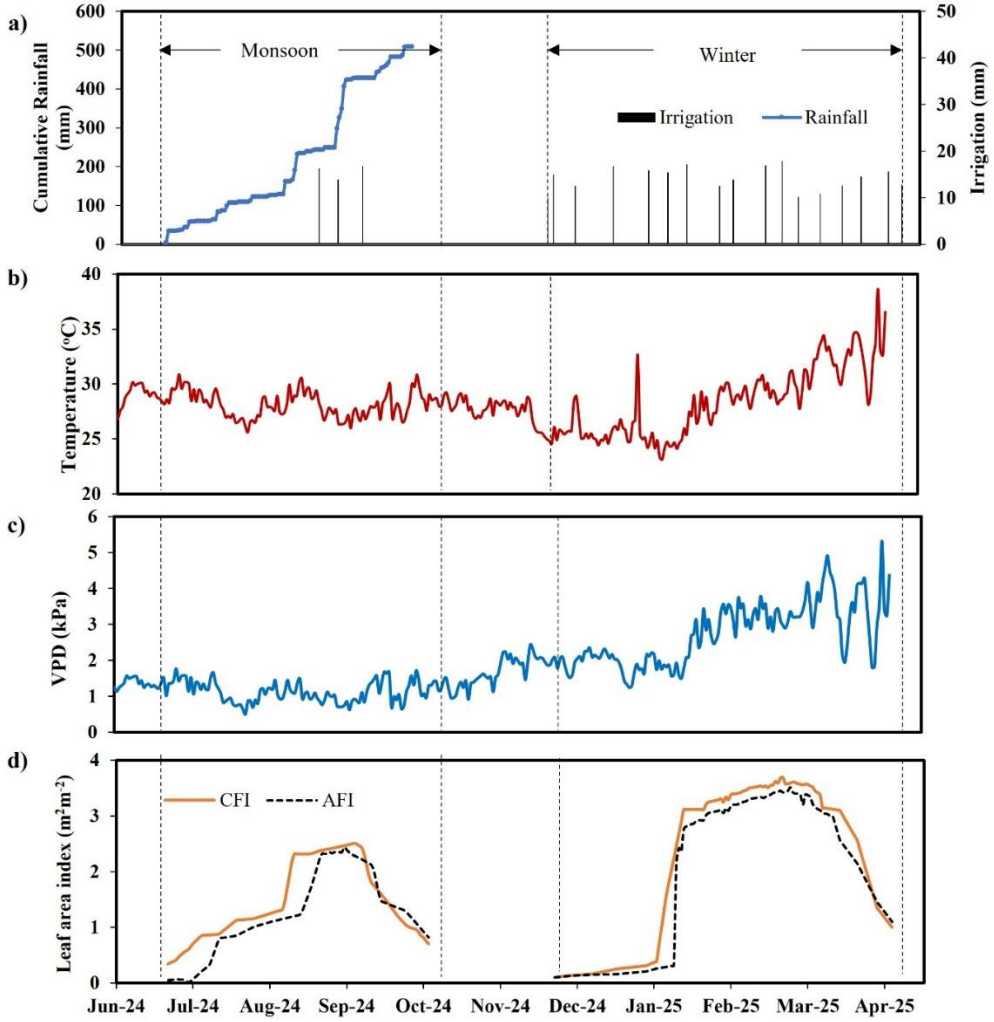
Table 2. Maize crop seasons with irrigation method, total rainfall and irrigation, sowing and harvest dates, crop length and maximum leaf area index (LAI) at Ind-IITH experimental site.

Crop season	Irrigation method	Rain [mm]	Irrigation [mm]	Sowing Date [DD/MM/YYYY]	Harvest Date [DD/MM/YYYY]	Crop length [Days]	Max LAI [m^2 m^{-2}]	Atmospheric evaporative demand ET_o [mm]

Monsoon	CFI	509	47	22/06/2024	05/10/2024	110	2.4	620
Monsoon	AFI	509	42	22/06/2024	05/10/2024	110	2.3	620
Winter	CFI	0	353.4	25/11/2024	10/04/2025	136	3.5	705
Winter	AFI	0	353.4	25/11/2024	10/04/2025	136	3.4	705

Variations in major meteorological variables in Figure 4 shows that, rainfall was predominantly concentrated during the monsoon season (June-August), totalling 509 mm, while three irrigation events, totalling 46.8 mm, were applied primarily during the dough (grain-filling) and maturity stages. Despite this additional input, the balance between total available water (precipitation + irrigation) and atmospheric evaporative demand (ET_o) remained negative, with deficits of -64 mm and -81 mm under CFI and AFI treatments, respectively. In contrast, the winter season received no rainfall, making the crop entirely dependent on irrigation, with total irrigation amounts of 543 mm under CFI and 453 mm under AFI. Despite these irrigation inputs, total available water remained below the ET_o, resulting in water deficits of -163 mm under CFI and -252 mm under AFI. Air temperature remained relatively stable during the monsoon (28.23 ± 1.20 °C), whereas during the winter season it increased progressively from 25.63°C to a peak of 38.63°C toward the end of the growing season. VPD variations closely followed temperature patterns, with mean values of 1.12 kPa and 2.73 kPa during the monsoon and winter seasons, respectively. Average LAI was lower during the monsoon (1.33 m^2 m^{-2}) compared to winter (1.97 m^2 m^{-2}), likely influenced by

252 seasonal differences in radiation and atmospheric conditions. Overall, the monsoon period
253 exhibited relatively stable temperatures and lower VPD, whereas the winter season experienced
254 progressively increasing temperatures and substantially higher VPD, indicating greater
255 atmospheric water demand. In comparison, FR-Lam showed moderate year-to-year differences
256 in climate, whereas Ind-IITH exhibited a near-complete shift from water-abundant to water-
257 deficient conditions between two seasons, along with a marked increase in VPD.



258

259 **Figure 4.** Seasonal variations in environmental variables, including cumulative rainfall and Irrigation **(a)**; Air
260 temperature **(b)**; Vapor pressure deficit **(c)**; Leaf area index **(d)** observed at Ind-IITH experimental site during
261 maize growing seasons.

262

263 **2.2 Field measurements**

264 2.2.1 Eddy covariance and meteorological datasets

265 At the FR-Lam site, an eddy covariance (EC) system was installed at 3.65m above
266 ground level. The system comprised a three-dimensional sonic anemometer (CSAT-3;
267 Campbell Scientific Inc., USA) and an open-path infrared gas analyser (LI-7500; LI-COR Inc.,
268 USA). Turbulent fluxes of CO_2 and H_2O were measured at 20 Hz using a datalogger (CR3000;
269 Campbell Scientific Inc., USA) and subsequently averaged over a 30-minute interval. High-
270 frequency raw data were processed using the EdiRe software following the CarboEurope-IP
271 protocol (Aubinet et al., 1999) and the FLUXNET2015 processing guidelines (Pastorello et al.,
272 2020). After standard quality control procedures, net ecosystem exchange (NEE) was
273 calculated as the sum of turbulent CO_2 flux and the CO_2 storage within the canopy. NEE was
274 further partitioned into ecosystem respiration (R_{eco}) and gross primary productivity (GPP)
275 using the method proposed by Reichstein et al. (2005). This partitioning method had been
276 optimized for croplands by Béziat et al. (2010) (see also Pique et al. (2020) for further details).
277 Flux footprint estimates were derived using the analytical model of Kljun et al. (2004).
278 Meteorological variables, including net radiation (CNR1; Kipp & Zonen), wind speed and wind
279 direction (wind vane/propeller; R.M. Young), air temperature and relative humidity (HMP35;
280 Vaisala), precipitation (ARG100 rain gauge), and diffuse and total photosynthetic active
281 radiation (PAR) (BF3; Delta-T Devices Ltd., Cambridge, UK), were measured at a half-hourly
282 interval. The quality of the convective fluxes measured by the EC system was evaluated by
283 estimating energy balance closure (see Dare-Idowu et al. (2021)). Data points exhibiting poor
284 closure (< 0.3) were excluded from the dataset to ensure the reliability of the flux measurements
285 (Barr et al., 2006; Kidston et al., 2010). On average, 48% of the nighttime data was rejected
286 due to insufficient turbulence. A detailed description of the experimental setup and
287 instrumentation is provided in Béziat et al. (2010) and Dare-Idowu et al. (2021).

288 At the Ind-IITH site, both experimental fields were equipped with open-path eddy
289 covariance (EC) flux towers installed at a height of 2.2m above ground level. The EC system
290 consisted of an open-path infrared gas analyser (IRGASON-EB-NC; Campbell Scientific Inc.,
291 USA) coupled with a 3D sonic anemometer (EC100; Campbell Scientific Inc., USA) to
292 continuously measure of CO_2 and H_2O fluxes. High-frequency raw data were recorded at 10
293 Hz using dataloggers (CR3000 and CR1000X; Campbell Scientific Inc., USA) and
294 subsequently averaged to a 30-minute interval. Raw EC data were processed using EasyFlux-
295 PC software (Campbell Scientific Inc., USA). Detailed descriptions of data processing steps,
296 quality control procedures, and flux corrections are provided in Karimindla et al. (2024). Gap
297 filling of missing flux data was performed using the 'REddyProc' package in the open-source
298 'R' environment, following the method proposed by Reichstein et al. (2005). Net ecosystem
299 exchange (NEE) was calculated as the sum of turbulent CO_2 fluxes and the CO_2 storage within
300 the canopy and further partitioned into ecosystem respiration (R_{eco}) and gross primary
301 productivity (GPP) using the nighttime-based partitioning approach of Reichstein et al. (2005).
302 Flux footprint estimates were derived using the analytical model developed by Kljun et al.
303 (2004). Meteorological variables, including net radiation (CNR4; Campbell Scientific Inc.,
304 USA), air temperature and relative humidity (CS215 probe), wind speed and wind direction
305 (propeller wind monitor; R.M. Young), and precipitation (TE525-L rain gauge; Campbell
306 Scientific Inc., USA), were measured at 30-minute intervals. Similar to FR-Lam, datapoints
307 exhibiting poor closure (< 0.3) were excluded from the dataset to ensure the reliability of the
308 flux measurements (Barr et al., 2006; Karimindla et al., 2024; Kidston et al., 2010).
309
310 2.2.2 Vegetation characteristics and irrigation inputs
311 At the FR-Lam site, vegetation leaf area index (LAI) was monitored during the peak
312 growth period using a leaf area meter (LI-3100; LI-COR, Lincoln, NE, USA), following the

methodology described by Claverie et al. (2012). In addition, vegetation height (h_{veg}) and aboveground biomass were measured on site from field sub-sampling and compared to the yield provided by the farmer. Information on irrigation timing and applied water amounts was collected through regular farmer surveys. A comprehensive description of vegetation monitoring protocols and management practices is provided in Dare-Idowu et al. (2021) and Pique et al. (2020). At the Ind-IITH site, LAI was measured from the tasselling to harvest stages using a plant canopy analyser (LI-2200C; LI-COR, Lincoln, NE, USA) and vegetation height was measured manually using a graduated ruler. Aboveground biomass and grain yield were determined at harvest from field sampling. Irrigation timing and applied water amounts were recorded on a daily basis for both CFI and AFI treatments.

2.3 ISBA-A-g_s model description and implementation

The standard version of ISBA represents land surface heterogeneity using nineteen generic land cover types or patches: bare soil, rocks, ice and permanent snow, needleleaf trees, evergreen broadleaf trees, deciduous broadleaf trees, C3 crops, C4 crops, irrigated crops, herbaceous vegetation, tropical herbaceous vegetation, and wetlands (Calvet et al., 1998; Noilhan and Planton, 1989). In this study, ISBA was applied at a field scale (for which the cover is assumed to be homogeneous), and a single grid cell is characterized by a single dominant surface type (Noilhan and Planton, 1989). ISBA is implemented within the open-source SURFace EXternalisée (SURFEX) platform (version 9.1), developed by the Centre National de Recherches Météorologiques (CNRM) at Météo-France (Masson et al., 2013). In its standard configuration, leaf stomatal conductance is parameterized using the empirical approach of Jarvis (1976), which relies on multiplicative stress functions. While computationally efficient, this formulation has limitations in explicitly representing the physiological coupling between photosynthesis and stomatal regulation and doesn't account

for the direct effects of atmospheric CO_2 concentration on carbon assimilation and stomatal conductance. To overcome these limitations, ISBA was revised by Calvet et al. (1998) through the incorporation of an optional photosynthesis-based stomatal conductance scheme, commonly referred to as the 'A-g_s' model, originally proposed by Jacobs et al. (1996). In the Jacobs formulation, leaf-level carbon assimilation and stomatal conductance are simulated through a sequence of steps (described in Appendix A of Calvet et al. (1998) and Rivalland et al. (2005), with the net assimilation rate (A_m) and stomatal conductance (g_s) expressed as:

$$A_m = A_{m,max}\left[1 - \exp\left(-\frac{g_m^*(C_i - \Gamma)}{A_{m,max}}\right)\right] \quad (1)$$

$$g_s = 1.6\, g_{sc} + g_c \quad (2)$$

where $A_{m,\max}$(mg m^{-2} s^{-1}) is the maximum photosynthetic rate, Γ(µmol mol^{-1}) is the CO_2 compensation concentration, g_m^* (m s^{-1}) is the unstressed mesophyll conductance, C_i(µmol mol^{-1}) is the intercellular CO_2 concentration, g_s (m s^{-1}) is the stomatal conductance, g_{sc} (m s^{-1}) is the stomatal conductance to carbon and g_c (m s^{-1}) is the cuticular conductance. Typical values of $A_{m,\max}$for C3 and C4 crops, data are provided in Calvet (2000)

Radiative transfer scheme is applied to upscale these carbon and water fluxes to the canopy scale, following the approaches of Jacobs et al. (1996) and Roujean (1996). At the canopy level, gross primary productivity (GPP; gC m^{-2} s^{-1}) and evapotranspiration (ET; kg H_2O m^{-2} s^{-1}) are simulated, and water use efficiency (WUE; gC kg H_2O^{-1}) is then computed as a ratio of GPP to ET on a daily scale:

$$\text{WUE (gC kg } H_2O^{-1}) = \frac{\text{GPP}}{\text{ET}} \quad (3)$$

In this study, the non-interactive vegetation option of ISBA-A-g_s is employed, the key vegetation characteristics: LAI, vegetation height (h_{veg}), and fractional vegetation cover (F_C) are prescribed using *in situ* measurements rather than simulated dynamically. The multilayer soil diffusion (DIF) scheme is adopted to simulate vertical transfers of soil moisture and heat

within the soil profile (Decharme et al., 2026). The main input parameters and state variables used in the model simulations for the FR-Lam and Ind-IITH sites are summarized in Table S1-S2, respectively. At both sites, vegetation characteristics including LAI, h_{veg}, and F_c were prescribed from in-situ measurements at 10-day intervals. Surface roughness length was estimated as a fixed fraction of canopy height ($0.15 \times h_{veg}$). In this study, patch 8, representing C4 crops, was employed to simulate the maize crop at both sites. The model was forced with half-hourly meteorological observations, including air temperature (TA, K), specific humidity (QA, kg kg^{-1}), surface air pressure (PS, Pa), incoming longwave radiation (LWin, W m^{-2}), wind speed (WS, m s^{-1}), wind direction (degrees), ambient CO_2 concentration (kg m^{-3}), rainfall (RAIN, kg m^{-2}), and incoming shortwave radiation (SWin, W m^{-2}). The multilayer soil diffusion scheme requires information on soil stratification; accordingly, soil layers at depths of 0, 5, 10, 30, 50, 100, and 150 cm below the ground surface were considered. Soil hydraulic conductivity was estimated using pedotransfer functions based on measured sand and clay contents at the respective depths (Cosby et al., 1984). Initial soil moisture and soil temperature profiles were prescribed using in-situ observations. Surface albedo during active sunshine hours (10:00-15:00 local time) is provided to minimize the influence of low solar zenith angles, following Kalma and Stanhill (1969). Subsequently, total surface albedo was partitioned into soil (alb_{soil}) and vegetation (alb_{veg}) components using a fractional weighting approach based on F_C. Model simulations were constrained to the crop growth period by prescribing site-specific sowing and harvesting dates in the forcing files.

2.4 Model calibration and validation

To achieve an optimal balance between the large number of input parameters in ISBA-A-g_s and the available computational resources, a stepwise calibration strategy was adopted. Based on previous studies and expert knowledge of the model, twelve parameters (gm, GC,

F2I, RE25, D_{Max}, CV, LAI_{Min}, R_{GL}, RSMIN, WR_{Max}, and Z_o-Z_H) that potentially influence GPP and ET simulations were initially selected (Aouade et al., 2020; Boone et al., 2017; Dare-Idowu et al., 2021). A one-at-a-time (OAT) sensitivity analysis was first performed by varying each parameter independently while keeping all other parameters fixed. For each parameter, 50 simulations were conducted across its predefined range for each calibration dataset. Model performance was evaluated by comparing simulated GPP, ET, and WUE against in-situ observations using the root mean square error (RMSE) and coefficient of determination (R^2). Parameter sensitivity was assessed using a Pareto-based multi-objective framework, with RMSE and R^2 as the objective functions (Demarty et al., 2005), followed by the Kolmogorov-Smirnov (KS) test to quantify the statistical separation between acceptable and non-acceptable parameter sets. The OAT sensitivity analysis was then used to identify the most influential parameters. No automated optimization algorithm was employed. Instead, the sensitive parameters were manually refined through an iterative trial-and-error procedure, in which parameter values were progressively adjusted within their physically realistic ranges. Model simulations were repeatedly evaluated until further improvements in RMSE and R^2 became negligible while maintaining physically realistic parameter values. For the FR-Lam site, calibration was performed using the 2008, 2010, and 2012 growing seasons, and the optimized parameter set was independently validated using the 2006, 2014, and 2015 growing seasons. At the Ind-IITH site, owing to the availability of only one year of observations (monsoon and winter seasons under CFI and AFI), treatment-specific parameter sets were calibrated separately for each irrigation treatment and season. Independent temporal validation was therefore not feasible for the Ind-IITH site, and model transferability across contrasting hydro-climatic conditions was evaluated primarily through comparison with the independently validated FR-Lam simulations.

412 **2.5 Model assessment**

413 Model performance in reproducing GPP, ET, and WUE was evaluated using three
414 goodness-of-fit indicators. EC flux-tower measurements were used as the reference for model
415 validation. The selected indicators quantify the strength of association, residual errors, and
416 systematic bias between observations and simulations. These metrics were computed using
417 paired EC-observed values (O_i) and ISBA-A-g_s simulated values (P_i) of GPP, ET, and WUE,
418 along with their respective means ($\bar{O}$ and $\bar{P}$), during crop growth seasons. Model performance
419 was assessed using the coefficient of determination (R^2), the root means square error (RMSE),
420 and the percentage bias (PBIAS).

421 i. The coefficient of determination (R^2) quantifies the strength of the linear association
422 between observed and simulated fluxes:

423 $$R^2 = \left\{ \frac{\sum_{i=1}^{n}(O_i-\bar{O})(P_i-\bar{P})}{[\sum_{i=1}^{n}(O_i-\bar{O})^2]^{0.5}\,[\sum_{i=1}^{n}(P_i-\bar{P})^2]^{0.5}} \right\}^2 \quad (4)$$

424 ii. RMSE provides a measure of the overall magnitude of simulation errors.

425 $$RMSE = \left[\frac{1}{n}\sum_{i=1}^{n}(P_i - O_i)^2\right]^{0.5} \quad (5)$$

426 iii. PBIAS indicates the average tendency of the model to overestimate or underestimate the
427 observed values.

428 $$PBIAS = 100\,\frac{\sum_{i=1}^{n}(O_i - P_i)}{\sum_{i=1}^{n} O_i} \quad (6)$$

429 To further perform diagnostic analysis, the slope of $GPP \cdot VPD^{0.5}$ -ET relationship called as
430 underlying water use efficiency (uWUE) was examined using both observations and model
431 simulations. This analysis was restricted to periods of peak leaf area index (LAI > 1.5 $m^2\ m^{-2}$)
432 to minimize soil evaporation contributions and isolate canopy-level stomatal behaviour.
433 Additionally, the response of evaporative fraction ($EF = \frac{LE}{H+LE}$) to VPD was analysed using half-
434 hourly averages during peak photosynthetic periods (11:00-15:00) within the active growing

435 phase to assess the ability of the ISBA-A-g_s model to capture land-atmosphere coupling and
436 surface energy partitioning under contrasting irrigation and hydro-climatic conditions.
437
438 **3.0 Results**
439 **3.1 Dynamics of GPP, ET, and WUE**
440 Figure 5 presents seasonal variations in GPP, ET, and WUE, highlighting the substantial
441 interannual variability at FR-Lam, and treatment-specific differences at Ind-IITH. At FR-Lam,
442 seasonal mean GPP ranged from 8 to 11 gC m^{-2} day^{-1}, with the strongest carbon uptake
443 observed in 2015 and comparatively lower GPP in 2010, corresponding to the wet and dry
444 growing seasons, respectively. Similarly, ET displayed considerable interannual variability,
445 with 2015 showing the highest upper whisker and 2008 the lowest, suggesting large differences
446 in seasonal evaporative demand and canopy water fluxes. In contrast, WUE exhibited an
447 inverse pattern, with the highest values recorded in 2008, whereas 2010 and 2015 showed
448 comparatively lower WUE. Despite relatively high GPP in 2012, WUE remained moderate
449 because the increase in carbon uptake was accompanied by a concurrent increase in ET.
450 At Ind-IITH, GPP exhibited overlapping interquartile ranges between the CFI and AFI
451 treatments during both the monsoon and winter seasons, indicating broadly similar patterns of
452 ecosystem carbon assimilation despite differences in irrigation management. Nevertheless,
453 relative to CFI, AFI reduced seasonal GPP by 18.78% during the monsoon and 17.06% during
454 the winter. In contrast, AFI substantially reduced ecosystem ET by 28.79% during the monsoon
455 and by 41.87% during the winter compared with CFI. Consequently, WUE increased by
456 42.46% during the monsoon and 40.10% during the winter under AFI, primarily because the
457 reduction in ET was proportionally greater than the reduction in GPP. In addition, grain yields
458 under CFI and AFI were 6.08 and 4.82 quintals, respectively, corresponding to a yield reduction
459 of 15-20% under AFI. However, AFI required nearly 40-45% less irrigation water than CFI,

460 resulting in a 15-30% improvement in agronomic WUE and demonstrating a favourable trade-
461 off between water conservation and crop productivity. These findings suggest that, although
462 AFI imposed a moderate yield penalty, the substantial water savings and enhanced ecosystem
463 WUE make it a promising irrigation strategy for sustainable maize production in semi-arid
464 regions, where maximizing water productivity is often more important than maximizing yield.
465 Overall, the results indicate that irrigation management exerted a stronger influence on
466 ecosystem ET than on GPP, thereby enhancing WUE at the Ind-IITH site.

467 A cross-site comparison further highlights that WUE variability is governed by different
468 mechanisms at the FR-Lam and Ind-IITH sites, despite exhibiting broadly comparable
469 magnitudes. At FR-Lam, WUE was primarily controlled by interannual climatic variability,
470 with higher values observed during drier years (e.g. 2008) and lower WUE observed in wet
471 year (e.g. 2015). In contrast, at Ind-IITH, WUE was more strongly influenced by irrigation
472 management than by seasonal carbon assimilation, with AFI consistently enhancing WUE
473 relative to CFI. Despite these contrasting controls, the overall range of WUE remained broadly
474 similar between the temperate and semi-arid environments, indicating that both climatic
475 variability and irrigation management can produce comparable ecosystem-scale WUE's
476 through different underlying mechanisms.

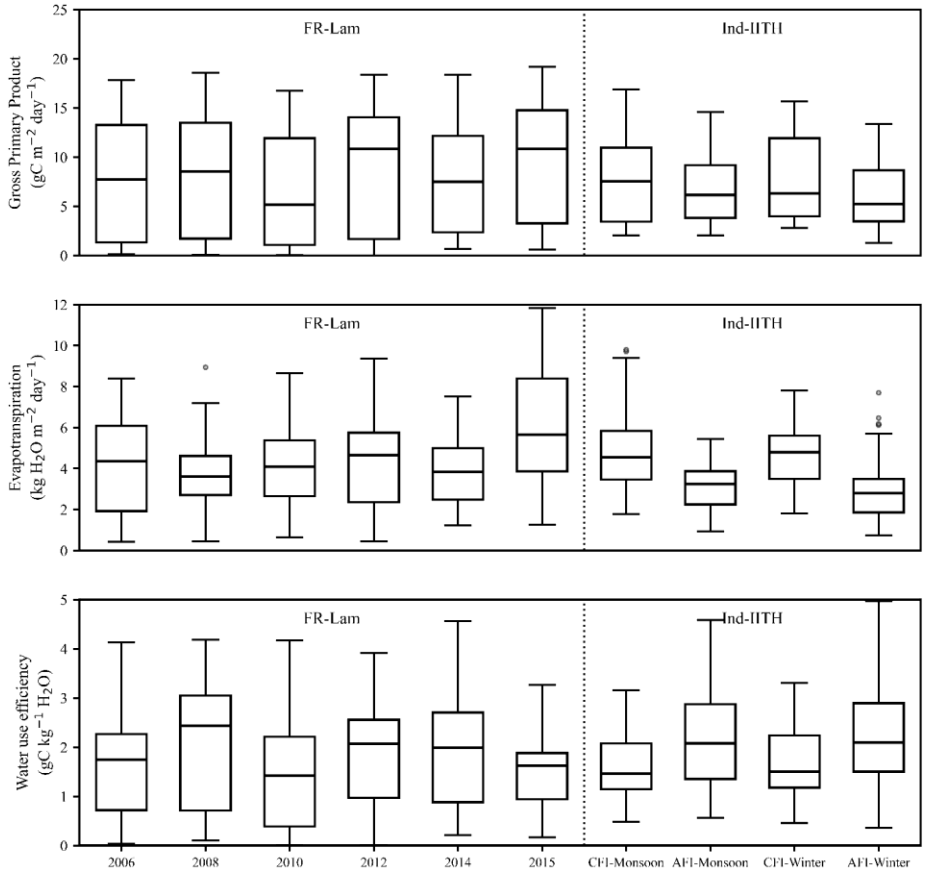


Figure 5. Seasonal variability of gross primary productivity (GPP), evapotranspiration (ET), and water use efficiency (WUE) during six maize growing seasons (2006, 2008, 2010, 2012, 2014, and 2015) at the FR-Lam site and four treatments considered at the Ind-IITH site.

3.2 Model calibration

Table 3 summarizes the calibrated optimal parameter estimates of the ISBA-A-g_s model for the FR-Lam. Among the 12 parameters investigated, five parameters (gm, GC, F2I, RE25, and D_{Max}) were identified as particularly sensitive. Results shows that the reduction in mesophyll conductance (gm) from its initial value indicates greater internal CO_2 diffusion limitations, reflecting stronger mesophyll constraints on carbon assimilation under contrasting environmental conditions. The optimized upper-bound value of cuticular conductance (GC) indicates a substantial contribution of cuticular water loss to total transpiration, particularly during dry periods. The optimized F2I parameter suggests that soil moisture stress begins to constrain carbon-water flux coupling, reflecting moderate drought sensitivity of the ecosystem.

The converged values of RE25 and D_{Max} indicate stable temperature-normalized respiratory fluxes and enhanced stomatal sensitivity to atmospheric VPD, supporting the observed regulation of transpiration under dry atmospheric conditions. Overall, the calibrated parameters indicate that the FR-Lam site is characterized by relatively high cuticular conductance and strong atmospheric control of stomatal behaviour.

Table 3. Calibrated ISBA-A-g_s model parameters for the FR-Lam experimental site.

Description	Symbol	Initial value considered	Optimal Value	Reference
Mesophyll conductance	gm	7.53×10^{-3}	2×10^{-3}	(Calvet, 2000)
Cuticular conductance	GC	4×10^{-4}	4.2×10^{-4}	(Gibelin et al., 2006)
Critical normalized soil water content for stress parameterization	F2I	2.0×10^{-1}	3.34×10^{-1}	(Calvet, 2000)
Ecosystem respiration parameter	RE25	2.88×10^{-7}	2.50×10^{-7}	(Gibelin et al., 2006)
Maximum leaf to air saturation deficit	D_{Max}	5.0×10^{-2}	6.5×10^{-2}	(Calvet, 2000)

Table 4 summarizes the calibrated optimal parameter estimates of the ISBA-A-g_s model at the Ind-IITH site. Among the 12 parameters investigated, five (gm, GC, F2I, RE25, and D_{Max}) were identified as particularly sensitive. Results show that the lower value of optimal mesophyll conductance (gm) under AFI during the monsoon reflected stronger internal CO_2 diffusion limitations, leading to a minimal reduction in GPP while reducing ET to a greater extent, thereby enhancing WUE. In contrast, slightly higher gm during AFI in winter favoured carbon assimilation under given atmospheric demand. The calibrated GC values remained low across all treatments, with marginally higher values under CFI during winter, indicating greater cuticular water loss under fully irrigated conditions. The calibrated F2I values in AFI were

observed to be higher during winter, indicating stronger soil moisture control on stomatal regulation under dry conditions and promoting earlier reductions in transpiration. The parameters such as RE25 and D_{Max} showed marginal variations across treatments, indicating seasonal changes in respiration and moderate atmospheric control that reduced ET under high VPD while maintaining stable WUE. Overall, the calibrated parameters under AFI indicated subtle reductions in mesophyll conductance and soil moisture stress thresholds, reflecting physiological optimization under alternate wetting and drying conditions in the semi-arid agroecosystem. These optimized parameter values improved the representation of GPP, ET, and WUE, reducing model bias and enhancing agreement between simulated and observed fluxes (Table S3-S4). Together, these results demonstrate the capability of the ISBA-A-g_s model to mechanistically represent irrigation-driven ecosystem carbon-water interactions under contrasting temperate and tropical semi-arid hydro-climatic conditions within the scope of the available observations, which constitutes the principal scientific contribution of this study.

Table 4. Calibrated ISBA-A-g_s model parameters for the Ind-IITH experimental site.

Description	Symbol	Initial value considered	Optimal Value				References
			CFI - Monsoon	AFI - Monsoon	CFI - Winter	AFI - Winter	
Mesophyll conductance	gm	7.53×10^{-3}	2.5×10^{-3}	2.2×10^{-3}	2.8×10^{-3}	2.7×10^{-3}	(Calvet, 2000)
Cuticular conductance	GC	4×10^{-4}	3×10^{-4}	2.9×10^{-4}	3.5×10^{-4}	3.2×10^{-4}	(Gibelin et al., 2006)

Critical normalized soil water content for stress parameterization	F2I	2.0×10^{-1}	4.0×10^{-1}	4.05×10^{-1}	4.12×10^{-1}	4.09×10^{-1}	(Calvet, 2000)
Ecosystem respiration parameter	RE25	2.88×10^{-7}	2.20×10^{-7}	2.22×10^{-7}	2.32×10^{-7}	2.40×10^{-7}	(Gibelin et al., 2006)
Maximum leaf to air saturation deficit	D_{Max}	4.0×10^{-2}	7.0×10^{-2}	7.1×10^{-2}	7.5×10^{-2}	7.1×10^{-2}	(Calvet, 2000)

3.3 Model performance

3.3.1 FR-Lam site

The calibrated ISBA-A-g_s model demonstrated strong capability in reproducing ecosystem GPP, ET, and WUE dynamics at the FR-Lam site (Figure 6). GPP was simulated with high accuracy (R^2 = 0.80-0.93), successfully capturing both dry (2008) and wet (2014) conditions, indicating a robust representation of photosynthetic processes across contrasting moisture conditions. Low RMSE and moderate PBIAS further confirmed reliable GPP estimates, although systematic overestimation was evident in 2014 (-28%) and 2015 (-16%), suggesting enhanced simulated carbon assimilation under non-water-limited conditions. ET simulations also showed moderate to strong agreement with observations (R^2 = 0.60-0.86), with the best performance during the wet year of 2015, reflecting improved representation of atmospheric demand and surface conductance. In contrast, larger RMSE and PBIAS during the dry year of 2008 (RMSE = 2.05 kg H_2O m^{-2} day^{-1}; PBIAS = -36.0%) indicate greater sensitivity to seasonal variations in soil moisture availability and evaporative demand. WUE exhibited

comparatively better performance (R^2 = 0.38-0.78); however, because it is derived from both GPP and ET, minor deviations in ET during 2015 propagated through the GPP/ET ratio, resulting in larger fluctuations in WUE (RMSE = 0.70 gC kg^{-1} H_2O; PBIAS = -12.9%). Overall, the calibrated ISBA-A-g_s model effectively captured ecosystem-scale carbon and water dynamics, with the strongest performance for GPP, robust simulation of ET, and comparatively greater uncertainty in WUE arising from propagated errors in GPP and ET.

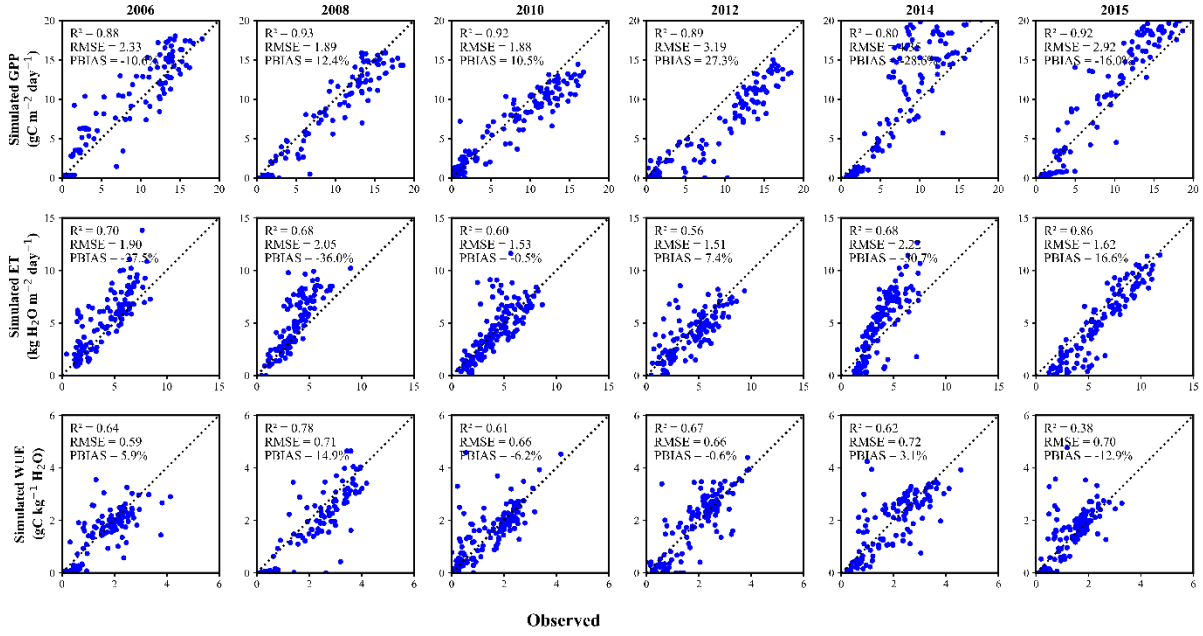


Figure 6. Scatter plots comparing daily eddy covariance observations with ISBA-A-g_s simulated gross primary productivity (GPP: first row), evapotranspiration (ET: second row), and water use efficiency (WUE: third row) at the FR-Lam site during six maize growing seasons (2006, 2008, 2010, 2012, 2014, and 2015). Statistical performance metrics, including the coefficient of determination (R^2), root mean square error (RMSE), and percentage bias (PBIAS), are reported in each panel.

The cumulative observed and simulated flux dynamics revealed pronounced interannual variability in seasonal GPP and ET at the FR-Lam site (Figure 7). Cumulative GPP ranged from 900 gC m^{-2} in 2008 to a peak of 1500 gC m^{-2} in 2015, corresponding to relatively dry and wet growing seasons, respectively. The steep increase in cumulative GPP during the peak growing period (May-August) reflected enhanced canopy photosynthesis associated with

maximum leaf area development. Accordingly, mean seasonal GPP accumulation rates (temporal slope of the cumulative curves) were highest in 2015 (observed: 11.61; simulated: 12.10 gC m^{-2} day^{-1}) and lowest in 2008 (observed: 9.11; simulated: 8.07 gC m^{-2} day^{-1}). Similarly, cumulative ET ranged from 500 kg H_2O m^{-2} in 2008 to a peak of 800 kg H_2O m^{-2} in 2015, reflecting the relatively dry and wet growing seasons, respectively. Mean seasonal ET accumulation rates were also highest in 2015 (observed: 6.73; simulated: 5.76 kg H_2O m^{-2}) and lowest in 2008 (observed: 3.80; simulated: 4.19 kg H_2O m^{-2}). Overall, the simulated cumulative GPP and ET closely reproduced the observed seasonal patterns, although slight overestimation of GPP was evident in 2014 and 2015 and deviations in cumulative ET occurred in 2008 and 2014, likely reflecting model sensitivity to atmospheric dryness. Nevertheless, the close agreement between simulated and observed cumulative fluxes demonstrates that the calibrated ISBA-A-g_s model effectively captured seasonal carbon and water dynamics at the FR-Lam site.

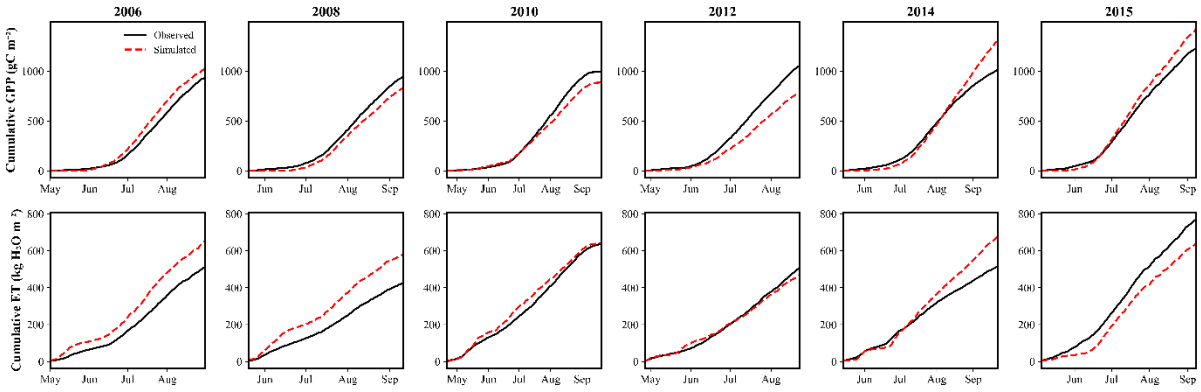
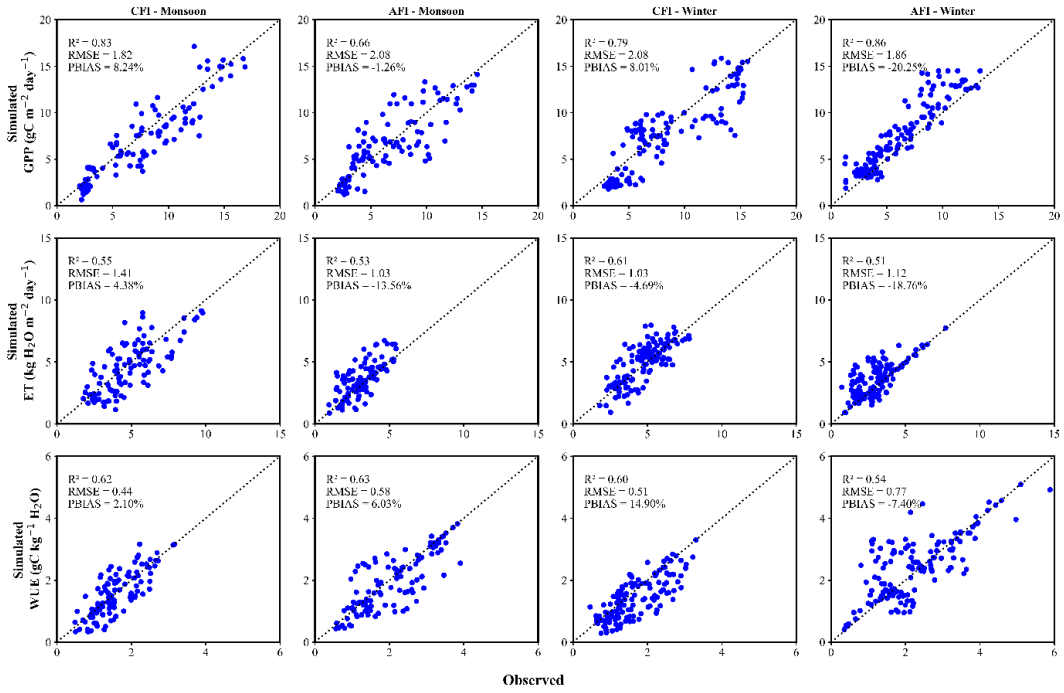


Figure 7. Cumulative plots by accumulating daily eddy covariance observations with ISBA-A-g_s simulated gross primary productivity (GPP: first row) and evapotranspiration (ET: second row) at the FR-Lam site during six maize growing seasons (2006, 2008, 2010, 2012, 2014, and 2015).

3.3.2 Ind-IITH site

The calibrated ISBA-A-g_s model showed robust performance in simulating GPP, ET, and WUE across both irrigation treatments and seasons at the Ind-IITH site (Figure 8). During the monsoon, GPP was accurately reproduced under both irrigation treatments, with better

performance under CFI (R^2 = 0.83) than AFI (R^2 = 0.66), while maintaining low model bias. During winter, GPP simulation improved further, particularly under AFI (R^2 = 0.86), although it was systematically overestimated. These results indicate that the model effectively captured seasonal photosynthetic dynamics, with slightly higher uncertainty under AFI during the monsoon due to the dominant influence of precipitation over irrigation. ET simulations showed moderate agreement across all treatments (R^2 = 0.51-0.61), with comparable performance during the monsoon and winter. However, ET was consistently overestimated under AFI, particularly during winter (PBIAS = -18.76%), indicating greater uncertainty under water-limited conditions. During the monsoon, WUE was well reproduced under both irrigation treatments, with similar performance (R^2 = 0.62-0.63) and low overall model bias, although AFI showed slight underestimation than CFI. During winter, WUE performance remained consistent (R^2 = 0.60 for CFI and 0.54 for AFI), with PBIAS ranging from -7.40% to 14.90%. Overall, the calibrated ISBA-A-g_s model showed the strongest performance for GPP, followed by ET and WUE, reflecting the propagation of uncertainties from both GPP and ET simulations, while AFI introduced slightly greater variability in ET and WUE than CFI.



595 **Figure 8.** Scatter plots comparing daily eddy covariance observations with ISBA-A-g_s simulated gross primary
596 productivity (GPP: first row), evapotranspiration (ET: second row), and water use efficiency (WUE: third row) at
597 the Ind-IITH site during four maize treatments considered. Statistical performance metrics, including the
598 coefficient of determination (R^2), root mean square error (RMSE), and percentage bias (PBIAS), are reported in
599 each panel.
600

601 The cumulative seasonal patterns reveal clear contrasts in GPP and ET between
602 irrigation treatments and crop seasons at the Ind-IITH site (Figure 9). Mean seasonal GPP
603 accumulation rates (temporal slope of the cumulative curves) were consistently higher under
604 CFI than AFI during both the monsoon (observed: 8.90 vs. 7.82; simulated: 8.21 vs. 7.68 gC
605 m^{-2} day^{-1}) and winter (observed: 8.89 vs. 6.94; simulated: 8.04 vs. 8.32 gC m^{-2} day^{-1}), although
606 the model slightly overestimated carbon uptake under AFI during the winter growing season,
607 particularly during the late reproductive stage. Additionally, the steeper mid-season slope
608 (January-March) reflects enhanced radiation availability and sustained canopy activity during
609 winter. Mean seasonal ET accumulation rates were consistently higher under CFI than AFI
610 during both the monsoon (observed: 4.97 vs. 3.25; simulated: 4.66 vs. 3.74 kg H_2O m^{-2} day^{-1})
611 and winter (observed: 4.80 vs. 3.02; simulated: 5.10 vs. 3.68 kg H_2O m^{-2} day^{-1}), with a more
612 pronounced divergence between irrigation treatments during winter, indicating greater
613 sensitivity of ET to irrigation management under drier atmospheric conditions. Overall, the
614 close agreement between observed and simulated cumulative GPP and ET demonstrates the
615 capability of the ISBA-A-g_s model to represent seasonal carbon assimilation and
616 evapotranspiration dynamics across the contrasting irrigation treatments and crop seasons.

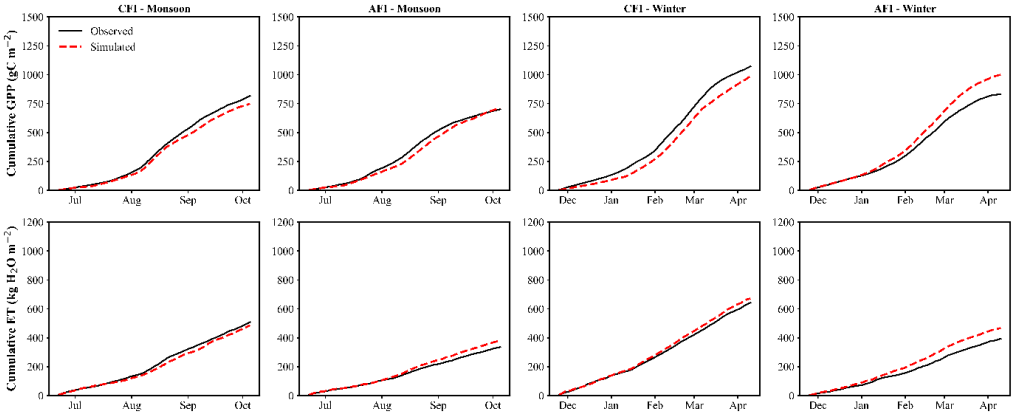


Figure 9. Cumulative plots by accumulating daily eddy covariance observations with ISBA-A-g_s simulated gross primary productivity (GPP: first row) and evapotranspiration (ET: second row) at the Ind-IITH site for four maize treatments considered.

3.4 Diagnostic analysis

Figure 10 illustrates variations in underlying water use efficiency (uWUE: slope of the GPP·VPD$^{0.5}$-ET relationship) at the FR-Lam and Ind-IITH sites, where steeper slopes indicate greater carbon gain per unit water loss through stronger stomatal regulation. At FR-Lam, observed uWUE ranged from 14.44 gC hPa$^{0.5}$ kg^{-1} H_2O in 2008 to 10.15 gC hPa$^{0.5}$ kg^{-1} H_2O in 2014, corresponding to relatively dry and wet years, respectively. The ISBA-A-g_s model closely reproduced this interannual variability, with simulated slopes differing by less than ±0.36 gC hPa$^{0.5}$ kg^{-1} H_2O from observations. At Ind-IITH, uWUE slopes were consistently steeper than those at FR-Lam, particularly during winter. During both seasons, observed uWUE was higher under AFI than CFI, suggesting stronger atmospheric control under alternate furrow irrigation. The ISBA-A-g_s model accurately reproduced these seasonal and treatment differences, with simulated slopes differing by less than ±0.74 gC hPa$^{0.5}$ kg^{-1} H_2O from observations, although slope magnitude was slightly underestimated under AFI. Overall, the steeper slopes at Ind-IITH relative to FR-Lam indicate stronger carbon-water coupling and greater ecosystem sensitivity to atmospheric demand under semi-arid tropical conditions.

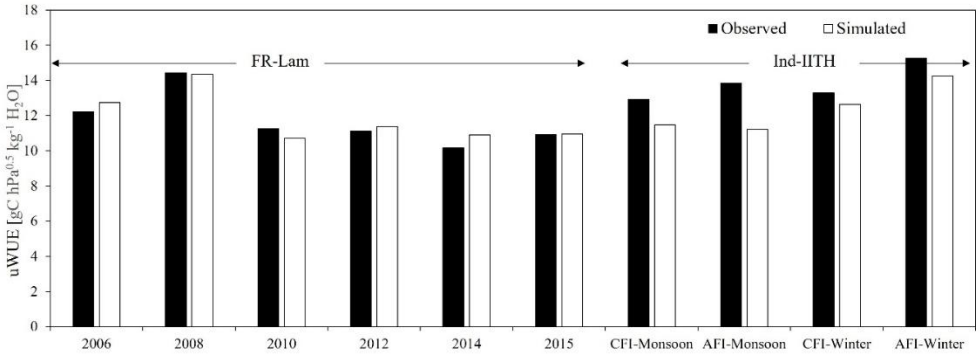


Figure 10. Seasonal variability in the underlying water use efficiency (uWUE) versus ET relationship at the FR-Lam and Ind-IITH sites. Solid bars represent observed EC estimates, while hatched bars denote ISBA-A-g_s simulated values.

The slope of the evaporative fraction (EF)-VPD relationship, which reflects the ecosystem-scale response of surface energy partitioning to atmospheric demand, is presented in Figure 11. At FR-Lam, observed EF-VPD slopes ranged from 0.0043 $hPa^{-0.5}$ in 2006 to 0.0086 $hPa^{-0.5}$ in 2015, with intermediate values in 2012 (0.0046 $hPa^{-0.5}$) and 2014 (0.0072 $hPa^{-0.5}$), corresponding to contrasting climatic conditions. The ISBA-A-g_s model closely reproduced this interannual variability, with simulated slopes differing by only 0.001-0.0015 $hPa^{-0.5}$ from observations. At Ind-IITH, EF-VPD slopes were consistently higher under CFI than AFI during both the monsoon (0.0061 vs. 0.0021 $hPa^{-0.5}$) and winter (0.0069 vs. 0.0025 $hPa^{-0.5}$), representing a 60-65% reduction under AFI and indicating weaker land-atmosphere coupling under partial soil wetting. The ISBA-A-g_s model successfully reproduced these seasonal and treatment-dependent differences, with only slight underestimation of the slope under winter CFI conditions. Overall, the positive EF-VPD slopes confirm the dominant influence of VPD on surface energy partitioning during peak canopy development. The higher slopes observed during the wetter years at FR-Lam and under CFI at Ind-IITH indicate stronger land-atmosphere coupling under moisture-sufficient conditions, whereas the reduced slopes under AFI reflect a moderated evaporative response associated with partial soil drying. Interestingly, the enhanced EF-VPD slopes observed at the FR-Lam site during 2014-2015 may

also be attributed to the change in maize cultivar, which promoted greater canopy development and higher LAI. Overall, the ISBA-A-g_s model successfully reproduced ecosystem carbon-water coupling and surface energy partitioning in response to contrasting irrigation treatments across the two study sites.

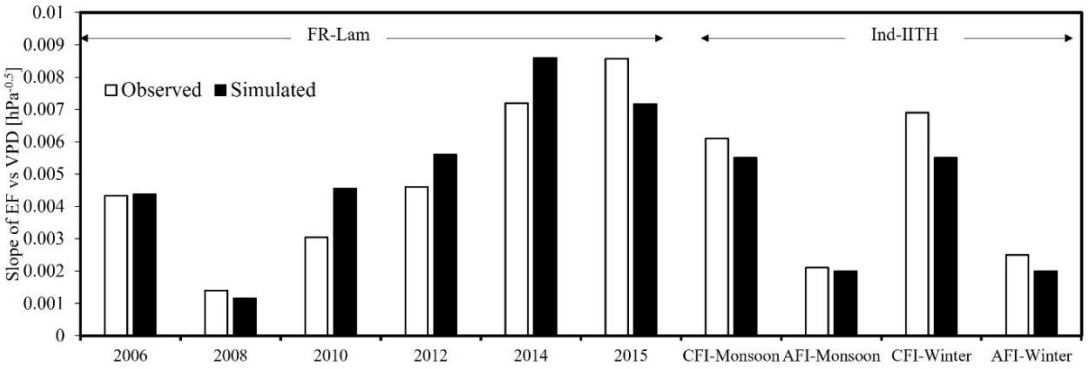


Figure 11. Variability in the slope of the EF vs VPD relationship at the FR-Lam and Ind-IITH sites. Solid bars represent observed EC estimates, and hatched bars denote ISBA-A-g_s simulated values.

4.0 Discussion

The calibrated ISBA-A-g_s framework demonstrated robust performance in reproducing the magnitude and seasonal dynamics of GPP, ET, and WUE across the temperate FR-Lam and semi-arid Ind-IITH sites, demonstrating its ability to represent coupled carbon-water processes under contrasting hydro-climatic conditions. The calibrated parameter sets further revealed distinct ecosystem functioning between the two sites. Higher values of GC and D_{Max} at FR-Lam (Table 3) indicate stronger regulation by atmospheric demand, whereas higher values of gm and F2I at Ind-IITH (Table 4) reflect greater sensitivity to irrigation management and soil moisture availability. These contrasting parameter responses are consistent with the differing climatic regimes and water management practices at the two sites, highlighting the ability of ISBA-A-g_s to realistically represent site-specific ecohydrological processes governing ecosystem carbon assimilation and water use.

At both sites, ISBA-A-g_s better performed in simulating GPP than ET, consistent with previous evaluations of land surface models. This performance difference may reflect the stronger constraints on photosynthetic processes compared with evapotranspiration, which is more sensitive to uncertainties in soil moisture dynamics and surface conductance parameterization (Best et al., 2011; Bonan et al., 2011). The strong agreement in daily and seasonal GPP indicates that the Jacob's-based photosynthesis scheme effectively represents radiation-driven carbon assimilation across varying moisture conditions. In contrast, the larger uncertainties in ET, particularly during years with irregular precipitation (e.g., 2012), highlight the sensitivity of evapotranspiration to soil water stress and land-atmosphere coupling (Dare-Idowu et al., 2021; De Kauwe et al., 2013; Moharana et al., 2025). Consequently, WUE exhibited greater variability because small ET errors propagated into the GPP/ET ratio, consistent with previous studies (Medlyn et al., 2011; Zhou et al., 2014). At the Ind-IITH site, ISBA-A-g_s successfully reproduced carbon assimilation and water fluxes under contrasting irrigation regimes. As at the FR-Lam site, GPP was simulated more accurately than ET, whereas the comparatively lower performance under AFI, particularly for ET during winter, reflects the increased complexity of representing partial root-zone drying, heterogeneous soil moisture distribution, and dynamic stomatal responses under deficit irrigation (Chintala et al., 2026; Chintala and Kambhammettu, 2026; Kang et al., 2001; Tardieu et al., 2015). Consequently, small ET biases propagated into WUE estimates despite the robust simulation of GPP. Importantly, the contrasting responses between CFI and AFI demonstrate that irrigation management can alter the balance between ecosystem carbon assimilation and water loss, thereby driving differences in WUE. Across the temperate FR-Lam and tropical semi-arid Ind-IITH sites, these results indicate that the ability of ISBA-A-g_s to reproduce WUE depends not only on its representation of photosynthesis and evapotranspiration individually, but also on its capacity to capture their coupled responses to soil moisture availability, atmospheric demand,

and irrigation management. Overall, the close agreement between observed and simulated daily, seasonal, and cumulative fluxes across both sites demonstrates that ISBA-A-g_s can reproduce the irrigation-driven carbon-water interactions underlying ecosystem WUE across contrasting hydro-climatic conditions. This highlights the value of a process-based land surface modelling framework for mechanistically evaluating how irrigation strategies modify ecosystem carbon-water coupling rather than simply quantifying their effects on individual carbon or water fluxes. The key scientific contribution of this study is therefore the application of a process-based land surface modelling framework to mechanistically evaluate the effects of contrasting irrigation strategies (CFI and AFI) on ecosystem carbon-water coupling and WUE, and how these effects vary between temperate and tropical semi-arid maize systems.

The consistently steeper uWUE slopes at the Ind-IITH site compared with FR-Lam indicate stronger carbon-water coupling under semi-arid conditions, where elevated VPD and limited soil water availability promote tighter stomatal regulation, resulting in relatively greater carbon gain per unit water loss (Medlyn et al., 2011; Zhou et al., 2014). The higher uWUE observed under AFI is consistent with enhanced intrinsic water use efficiency through partial root-zone drying and root-to-shoot chemical signalling, which reduce transpiration proportionally more than carbon assimilation, as reported in previous deficit-irrigation studies (Kang et al., 2001; Tardieu et al., 2015). In contrast, the higher EF-VPD slopes under CFI indicate stronger land-atmosphere coupling resulting from sustained latent heat flux under adequate soil moisture, whereas the substantially lower slopes under AFI demonstrate that partial soil drying reduced evaporation and transpiration, thereby weakening the sensitivity of surface energy partitioning to atmospheric demand (Seneviratne et al., 2010). Instead of observing these contrasting differences in between sites and irrigation treatments, the calibrated ISBA-A-g_s captured the underlying physiological processes regulating ecosystem carbon-water interactions across contrasting hydro-climatic conditions. The close agreement between

observed and simulated uWUE and EF-VPD relationships further demonstrates that the optimized site-specific parameterizations effectively represent climate-dependent physiological constraints on carbon assimilation, evapotranspiration, and surface energy partitioning.

5.0 Study limitations and future scope

Despite its robust performance, several limitations should be acknowledged. First, LAI was prescribed at 10-day intervals, which may be insufficient to capture the rapid canopy development and phenological transitions of maize, thereby introducing uncertainties in the simulation of ecosystem fluxes. Second, model calibration employed a one-at-a-time parameter optimization approach which, although computationally efficient, does not account for nonlinear interactions among model parameters. Third, the Ind-IITH analysis was based on a single agricultural year comprising monsoon and winter seasons under CFI and AFI treatments. Although this dataset encompasses a broad range of hydro-meteorological and irrigation conditions, it does not permit the assessment of interannual variability or independent model validation. Consequently, the findings for the Ind-IITH site should be interpreted within the scope of the available observations rather than as evidence of long-term model transferability across tropical semi-arid environments. Finally, contrasting hydro-climatic conditions across seasons (monsoon versus winter in India and wet versus dry years in France) introduce additional uncertainty in parameter transferability by altering radiation, VPD, and soil moisture regimes. Given that this study represents an initial evaluation, future research should assess the ISBA-A-g_s model using multi-year observations across diverse hydro-climatic conditions and irrigation management scenarios to better quantify interannual variability, parameter robustness, and long-term model transferability. In addition, incorporating higher-frequency vegetation dynamics (e.g., sub-weekly LAI and phenological updates) together with advanced

753 global optimization techniques (e.g., Monte Carlo or Bayesian calibration) would improve the
754 representation of parameter interactions, reduce calibration uncertainty, and further enhance
755 simulations of coupled carbon-water processes in maize agroecosystems.
756
757 **6.0 Conclusions**
758 This study investigated the ecosystem-scale dynamics of GPP, ET, and WUE of maize
759 under contrasting hydro-climatic conditions in a temperate (FR-Lam, France) and a tropical
760 semi-arid (Ind-IITH, India) ecosystems using the ISBA-A-g_s SVAT model within the SURFEX
761 land surface modelling framework. Driven by in-situ meteorological observations and
762 measured vegetation characteristics, the model was calibrated and validated to simulate
763 seasonal carbon-water fluxes. The major findings are summarized as follows:
764 1. At FR-Lam, interannual climatic variability primarily regulated GPP, ET, and WUE,
765 whereas irrigation management exerted a stronger control on ecosystem functioning at Ind-
766 IITH by substantially reducing ET while maintaining relatively stable carbon assimilation.
767 2. The calibrated parameter sets revealed that mesophyll conductance, stomatal regulation,
768 atmospheric demand, and soil moisture limitation differed systematically between climates
769 and irrigation treatments, demonstrating that site-specific calibration enables ISBA-A-g_s to
770 mechanistically represent ecosystem responses.
771 3. The calibrated ISBA-A-g_s model consistently achieved higher performance for GPP than
772 ET while realistically capturing the contrasting influences of climate variability and
773 irrigation management on ecosystem carbon and water fluxes, demonstrating its capability
774 under the hydro-climatic and management conditions.
775 4. The complementary uWUE and EF-VPD diagnostic analyses demonstrated that ISBA-A-
776 g_s captures the ecophysiological and hydrological mechanisms governing ecosystem
777 carbon-water interactions and land-atmosphere coupling processes.

Overall, this study demonstrates that ISBA-A-g_s provides a robust process-based framework for representing ecosystem carbon-water interactions under contrasting temperate (FR-Lam) and tropical semi-arid (Ind-IITH) hydro-climatic conditions. While the model successfully reproduced interannual variability at FR-Lam and seasonal irrigation-driven responses at Ind-IITH, the conclusions for the latter are restricted to the available observation period and should be interpreted as evidence of the model's capability under the evaluated irrigation and seasonal conditions alone.

Acknowledgements

The corresponding author thanks CEFIPRA for facilitating a research mobility to CESBIO, Toulouse, France, through the Raman Charpak Fellowship. The corresponding author also acknowledges the financial support provided by the Ministry of Education, Government of India, through the Prime Minister's Research Fellowship (PMRF) for the Grant Number PMRF/2002195. The corresponding author acknowledges Kanishka Mallick for his careful review of the manuscript and valuable guidance throughout the review process. The authors acknowledge undergraduate students of the College of Agriculture Engineering, Sangareddy, for helping during field experiments in India. Data acquisition for FR-Lam was funded by the Institut National des Sciences de l'Univers of the Centre National de la Recherche Scientifique through ICOS. Facilities and staff were also funded by the University of Paul Sabatier, CNES, and Institut de Recherche pour le Développement.

Author contribution

Syam Chintala: Experimentation, Data collection and curation, Methodology, Model setup simulations, Results Analysis, Investigation, Writing - Original draft. **Lionel Jarlan:** Results analysis, Writing - Original draft & editing, Project administration, Supervision. **Vincent**

Rivalland: Results Analysis and interpretation, and Writing - Original draft & review. **Aaron Boone:** Results analysis and Model setup. **Oluwakemi Dare-Idowu:** Data curation and Input data preparation. **Valerie Le Dantec:** Results interpretation and Writing - Original draft & review. **Gilles Boulet**: Results interpretation and Writing - Original draft & review. **BVN P. Kambhammettu**: Results analysis, Writing - Original draft & review, Project administration, Supervision. **Aurore Brut**: Results analysis, Writing - Original draft & review, Project administration, Supervision.

Code/Data availability

All the relevant datasets and input codes are available at: https://github.com/Chintalasyam/ISBA_Model.git

Competing Interests

The authors declare that they have no known competing financial interests or personal relationships that could have appeared to influence the work reported in this paper.

References

Al-Kayssi, A. A.: Role of alternate and fixed partial root-zone drying on water use efficiency and growth of maize (Zea mays L.) in gypsiferous soils, Int. Soil Water Conserv. Res., 11, 145–158, https://doi.org/10.1016/j.iswcr.2022.04.003, 2023.

Aouade, G., Jarlan, L., Ezzahar, J., Er-Raki, S., Napoly, A., Benkaddour, A., Khabba, S., Boulet, G., Garrigues, S., Chehbouni, A., and Boone, A.: Evapotranspiration partition using the multiple energy balance version of the ISBA-A-gs land surface model over two irrigated crops in a semi-Arid Mediterranean region (Marrakech, Morocco), Hydrol. Earth Syst. Sci., 24, 3789–3814, https://doi.org/10.5194/hess-24-3789-2020,

2020.

Aubinet, M., Grelle, A., Ibrom, A., Rannik, Ü., Moncrieff, J., Foken, T., Kowalski, A. S., Martin, P. H., Berbigier, P., and Bernhofer, C.: Estimates of the annual net carbon and water exchange of forests: the EUROFLUX methodology, in: Advances in ecological research, vol. 30, Elsevier, 113–175, 1999.

Baldocchi, D.: Measuring fluxes of trace gases and energy between ecosystems and the atmosphere – the state and future of the eddy covariance method, Glob. Chang. Biol., 20, 3600–3609, https://doi.org/https://doi.org/10.1111/gcb.12649, 2014.

Baldocchi, D., Falge, E., Gu, L., Olson, R., Hollinger, D., Running, S., Anthoni, P., Bernhofer, C., Davis, K., Evans, R., Fuentes, J., Goldstein, A., Katul, G., Law, B., Lee, X., Malhi, Y., Meyers, T., Munger, W., Oechel, W., U, K. T. P., Pilegaard, K., Schmid, H. P., Valentini, R., Verma, S., Vesala, T., Wilson, K., and Wofsy, S.: FLUXNET: A New Tool to Study the Temporal and Spatial Variability of Ecosystem-Scale Carbon Dioxide, Water Vapor, and Energy Flux Densities, Bull. Am. Meteorol. Soc., 82, 2415–2434, https://doi.org/10.1175/1520-0477(2001)082<2415:FANTTS>2.3.CO;2, 2001.

Barr, A. G., Morgenstern, K., Black, T. A., McCaughey, J. H., and Nesic, Z.: Surface energy balance closure by the eddy-covariance method above three boreal forest stands and implications for the measurement of the CO2 flux, Agric. For. Meteorol., 140, 322–337, https://doi.org/10.1016/j.agrformet.2006.08.007, 2006.

Battude, M., Al Bitar, A., Brut, A., Tallec, T., Huc, M., Cros, J., Weber, J.-J., Lhuissier, L., Simonneaux, V., and Demarez, V.: Modeling water needs and total irrigation depths of maize crop in the south west of France using high spatial and temporal resolution satellite imagery, Agric. Water Manag., 189, 123–136, 2017.

Beer, C., Ciais, P., Reichstein, M., Baldocchi, D., Law, B. E., Papale, D., Soussana, J. F., Ammann, C., Buchmann, N., Frank, D., Gianelle, D., Janssens, I. A., Knohl, A.,

Köstner, B., Moors, E., Roupsard, O., Verbeeck, H., Vesala, T., Williams, C. A., and Wohlfahrt, G.: Temporal and among-site variability of inherent water use efficiency at the ecosystem level, Global Biogeochem. Cycles, 23, 1–13, https://doi.org/10.1029/2008GB003233, 2009.

Best, M. J., Pryor, M., Clark, D. B., Rooney, G. G., Essery, R. L. H., Menard, C. B., Edwards, J. M., Hendry, M. A., Porson, A., and Gedney, N.: The Joint UK Land Environment Simulator (JULES), model description–Part 1: energy and water fluxes, Geosci. Model Dev., 4, 677–699, 2011.

Béziat, P., Rivalland, V., Jarosz, N., Ceschia, E., Boulet, G., and Gentine, P.: Crop evapotranspiration partitioning and comparison of different water use efficiency approaches, in: EGU General Assembly Conference Abstracts, 3394, 2010.

Bonan, G. B., Lawrence, P. J., Oleson, K. W., Levis, S., Jung, M., Reichstein, M., Lawrence, D. M., and Swenson, S. C.: Improving canopy processes in the Community Land Model version 4 (CLM4) using global flux fields empirically inferred from FLUXNET data, J. Geophys. Res. Biogeosciences, 116, 2011.

Boone, A., Samuelsson, P., Gollvik, S., Napoly, A., Jarlan, L., Brun, E., and Decharme, B.: The interactions between soil–biosphere–atmosphere land surface model with a multi-energy balance (ISBA-MEB) option in SURFEXv8–Part 1: Model description, Geosci. Model Dev., 10, 843–872, 2017.

Buckley, T. N.: Modeling stomatal conductance, Plant Physiol., 174, 572–582, 2017.

Calvet, J.-C.: Investigating soil and atmospheric plant water stress using physiological and micrometeorological data, Agric. For. Meteorol., 103, 229–247, https://doi.org/https://doi.org/10.1016/S0168-1923(00)00130-1, 2000.

Calvet, J.-C., Noilhan, J., Roujean, J.-L., Bessemoulin, P., Cabelguenne, M., Olioso, A., and Wigneron, J.-P.: An interactive vegetation SVAT model tested against data from six

878 contrasting sites, Agric. For. Meteorol., 92, 73–95, 1998.
879 Chen, Y., Ding, Z., Yu, P., Yang, H., Song, L., Fan, L., Han, X., Ma, M., and Tang, X.:
880 Quantifying the variability in water use efficiency from the canopy to ecosystem scale
881 across main croplands, Agric. Water Manag., 262, 107427,
882 https://doi.org/10.1016/j.agwat.2021.107427, 2022.
883 Chintala, S. and Kambhammettu, B. V. N. P.: Dynamics and drivers of maize (Zea mays L.)
884 water use efficiency at leaf and plant scales under partial root-zone drying irrigation
885 combined with mulching across two soil regimes, Irrig. Sci., 44, 83,
886 https://doi.org/10.1007/s00271-026-01123-3, 2026.
887 Chintala, S., Kambhammettu, B. V. N. P., Mandadi, A. R., Jatoth, V., and Mallick, K.: From
888 leaf, canopy to ecosystem: Multi-scale dynamics and drivers of maize water use
889 efficiency in semi-arid tropics, Agric. For. Meteorol., 389, 111432,
890 https://doi.org/https://doi.org/10.1016/j.agrformet.2026.111432, 2026.
891 Claverie, M., Demarez, V., Duchemin, B., Hagolle, O., Ducrot, D., Marais-Sicre, C., Dejoux,
892 J.-F., Huc, M., Keravec, P., and Béziat, P.: Maize and sunflower biomass estimation in
893 southwest France using high spatial and temporal resolution remote sensing data,
894 Remote Sens. Environ., 124, 844–857, 2012.
895 Cosby, B. J., Hornberger, G. M., Clapp, R. B., and Ginn, T.: A statistical exploration of the
896 relationships of soil moisture characteristics to the physical properties of soils, Water
897 Resour. Res., 20, 682–690, 1984.
898 Cowan, I. R. and GD, F.: Stomatal function in relation to leaf metabolism and environment.,
899 1977.
900 Dare-Idowu, O., Jarlan, L., Le-Dantec, V., Rivalland, V., Ceschia, E., Boone, A., and Brut, A.:
901 Hydrological Functioning of Maize Crops in Southwest France Using Eddy Covariance
902 Measurements and a Land Surface Model, Water, 13,

https://doi.org/10.3390/w13111481, 2021.

Decharme, B., Tzanos, D., Hardouin, L., Boone, A., Minvielle, M., and Le, P.: A process-based modeling of soil organic matter physical properties for land surface models - Part 2 : Global land surface simulations and mineral soil compaction adjustment, 1–54, 2026.

Demarty, J., Ottlé, C., Braud, I., Olioso, A., Frangi, J. P., Gupta, H. V, and Bastidas, L. A.: Constraining a physically based soil-vegetation-atmosphere transfer model with surface water content and thermal infrared brightness temperature measurements using a multiobjective approach, Water Resour. Res., 41, 2005.

Erenstein, O., Jaleta, M., Sonder, K., Mottaleb, K., and Prasanna, B. M.: Global maize production, consumption and trade: trends and R&D implications, Food Secur., 14, 1295–1319, https://doi.org/10.1007/s12571-022-01288-7, 2022.

FAO: The future of food and agriculture: Trends and challenges, FAO, 2017.

Gibelin, A., Calvet, J., Roujean, J., Jarlan, L., and Los, S. O.: Ability of the land surface model ISBA-A-gs to simulate leaf area index at the global scale: Comparison with satellites products, J. Geophys. Res. Atmos., 111, 2006.

Hoover, D. L., Abendroth, L. J., Browning, D. M., Saha, A., Snyder, K., Wagle, P., Witthaus, L., Baffaut, C., Biederman, J. A., Bosch, D. D., Bracho, R., Busch, D., Clark, P., Ellsworth, P., Fay, P. A., Flerchinger, G., Kearney, S., Levers, L., Saliendra, N., Schmer, M., Schomberg, H., and Scott, R. L.: Indicators of water use efficiency across diverse agroecosystems and spatiotemporal scales, Sci. Total Environ., 864, 160992, https://doi.org/https://doi.org/10.1016/j.scitotenv.2022.160992, 2023.

Ito, A. and Inatomi, M.: Use of a process-based model for assessing the methane budgets of global terrestrial ecosystems and evaluation of uncertainty, Biogeosciences, 9, 759–773, https://doi.org/10.5194/bg-9-759-2012, 2012.

Jacobs, C. M. J., Van den Hurk, B. M. M., and De Bruin, H. A. R.: Stomatal behaviour and

photosynthetic rate of unstressed grapevines in semi-arid conditions, Agric. For. Meteorol., 80, 111–134, 1996.

Jarvis, P.: The interpretation of the variations in leaf water potential and stomatal conductance found in canopies in the field, Philos. Trans. R. Soc. London. B, Biol. Sci., 273, 593–610, 1976.

Kalma, J. D. and Stanhill, G.: The radiation climate of an irrigated orange plantation, Sol. Energy, 12, 491–508, 1969.

Kang, S., Liang, Z., Hu, W., and Zhang, J.: Water use efficiency of controlled alternate irrigation on root-divided maize plants, Agric. Water Manag., 38, 69–76, https://doi.org/10.1016/S0378-3774(98)00048-1, 1998.

Kang, S., Zhang, L., Hu, X., Li, Z., and Jerie, P.: An improved water use efficiency for hot pepper grown under controlled alternate drip irrigation on partial roots, Sci. Hortic. (Amsterdam)., 89, 257–267, https://doi.org/10.1016/S0304-4238(00)00245-4, 2001.

Karimindla, A. R., Kumari, S., S R, S., Chintala, S., and P. Kambhammettu, B.: The role of time averaging of eddy covariance fluxes on water use efficiency dynamics of maize, Atmos. Meas. Tech., 17, 5477–5490, https://doi.org/10.5194/amt-17-5477-2024, 2024.

De Kauwe, M. G., Medlyn, B. E., Zaehle, S., Walker, A. P., Dietze, M. C., Hickler, T., Jain, A. K., Luo, Y., Parton, W. J., and Prentice, I. C.: Forest water use and water use efficiency at elevated CO2: A model-data intercomparison at two contrasting temperate forest FACE sites, Glob. Chang. Biol., 19, 1759–1779, 2013.

Kidston, J., Brümmer, C., Black, T. A., Morgenstern, K., Nesic, Z., McCaughey, J. H., and Barr, A. G.: Energy balance closure using eddy covariance above two different land surfaces and implications for CO2 flux measurements, Boundary-Layer Meteorol., 136, 193–218, https://doi.org/10.1007/s10546-010-9507-y, 2010.

Kljun, N., Calanca, P., Rotach, M. W., and Schmid, H. P.: A simple parameterisation for flux

953 footprint predictions, Boundary-Layer Meteorol., 112, 503–523, 2004.
954 Knorr, W. and Heimann, M.: Impact of drought stress and other factors on seasonal land
955 biosphere CO2 exchange studied through an atmospheric tracer transport model, Tellus
956 B, 47, 471–489, 1995.
957 Kottek, M., Grieser, J., Beck, C., Rudolf, B., and Rubel, F.: World map of the Köppen-Geiger
958 climate classification updated, 2006.
959 Li, F., Liang, J., Kang, S., and Zhang, J.: Benefits of alternate partial root-zone irrigation on
960 growth, water and nitrogen use efficiencies modified by fertilization and soil water
961 status in maize, Plant Soil, 295, 279–291, https://doi.org/10.1007/s11104-007-9283-8,
962 2007.
963 Martí, B., Groh, J., Canut, G., and Boone, A.: Implementation of a dry surface layer soil
964 resistance in two contrasting semi-arid sites with SURFEX-ISBA V9.0, Geosci. Model
965 Dev., 19, 1991–2021, https://doi.org/10.5194/gmd-19-1991-2026, 2026.
966 Masson, V., Le Moigne, P., Martin, E., Faroux, S., Alias, A., Alkama, R., Belamari, S., Barbu,
967 A., Boone, A., and Bouyssel, F.: The SURFEXv7. 2 land and ocean surface platform
968 for coupled or offline simulation of earth surface variables and fluxes, Geosci. Model
969 Dev., 6, 929–960, 2013.
970 Medlyn, B. E., Duursma, R. A., Eamus, D., Ellsworth, D. S., Prentice, I. C., Barton, C. V. M.,
971 Crous, K. Y., De Angelis, P., Freeman, M., and Wingate, L.: Reconciling the optimal
972 and empirical approaches to modelling stomatal conductance, Glob. Chang. Biol., 17,
973 2134–2144, 2011.
974 Moharana, S., Chintala, S., and Kambhammettu, B. P.: Modeling leaf and crop water use
975 efficiency of rainfed Cotton: Interplay of environmental and biophysical drivers, Agric.
976 Water Manag., 317, 109626, https://doi.org/10.1016/j.agwat.2025.109626, 2025.
977 Noilhan, J. and Planton, S.: A simple parameterization of land surface processes for

978 meteorological models, Mon. Weather Rev., 117, 536–549, 1989.
979 Pastorello, G., Trotta, C., Canfora, E., Chu, H., Christianson, D., Cheah, Y.-W., Poindexter,
980 C., Chen, J., Elbashandy, A., Humphrey, M., Isaac, P., Polidori, D., Reichstein, M.,
981 Ribeca, A., van Ingen, C., Vuichard, N., Zhang, L., Amiro, B., Ammann, C., Arain, M.
982 A., Ardö, J., Arkebauer, T., Arndt, S. K., Arriga, N., Aubinet, M., Aurela, M.,
983 Baldocchi, D., Barr, A., Beamesderfer, E., Marchesini, L. B., Bergeron, O., Beringer,
984 J., Bernhofer, C., Berveiller, D., Billesbach, D., Black, T. A., Blanken, P. D., Bohrer,
985 G., Boike, J., Bolstad, P. V, Bonal, D., Bonnefond, J.-M., Bowling, D. R., Bracho, R.,
986 Brodeur, J., Brümmer, C., Buchmann, N., Burban, B., Burns, S. P., Buysse, P., Cale,
987 P., Cavagna, M., Cellier, P., Chen, S., Chini, I., Christensen, T. R., Cleverly, J., Collalti,
988 A., Consalvo, C., Cook, B. D., Cook, D., Coursolle, C., Cremonese, E., Curtis, P. S.,
989 D'Andrea, E., da Rocha, H., Dai, X., Davis, K. J., Cinti, B. De, Grandcourt, A. de,
990 Ligne, A. De, De Oliveira, R. C., Delpierre, N., Desai, A. R., Di Bella, C. M., Tommasi,
991 P. di, Dolman, H., Domingo, F., Dong, G., Dore, S., Duce, P., Dufrêne, E., Dunn, A.,
992 Dušek, J., Eamus, D., Eichelmann, U., ElKhidir, H. A. M., Eugster, W., Ewenz, C. M.,
993 Ewers, B., Famulari, D., Fares, S., Feigenwinter, I., Feitz, A., Fensholt, R., Filippa, G.,
994 Fischer, M., Frank, J., Galvagno, M., Gharun, M., Gianelle, D., Gielen, B., Gioli, B.,
995 Gitelson, A., Goded, I., Goeckede, M., Goldstein, A. H., Gough, C. M., Goulden, M.
996 L., Graf, A., Griebel, A., Gruening, C., Grünwald, T., Hammerle, A., Han, S., Han, X.,
997 Hansen, B. U., Hanson, C., Hatakka, J., He, Y., Hehn, M., Heinesch, B., Hinko-Najera,
998 N., Hörtnagl, L., Hutley, L., Ibrom, A., Ikawa, H., Jackowicz-Korczynski, M., Janouš,
999 D., Jans, W., Jassal, R., Jiang, S., Kato, T., Khomik, M., Klatt, J., Knohl, A., Knox, S.,
1000 Kobayashi, H., Koerber, G., Kolle, O., Kosugi, Y., Kotani, A., Kowalski, A., Kruijt, B.,
1001 Kurbatova, J., Kutsch, W. L., Kwon, H., Launiainen, S., Laurila, T., Law, B., Leuning,
1002 R., Li, Y., Liddell, M., Limousin, J.-M., Lion, M., Liska, A. J., Lohila, A., López-

Ballesteros, A., López-Blanco, E., Loubet, B., Loustau, D., Lucas-Moffat, A., Lüers, J., Ma, S., Macfarlane, C., Magliulo, V., Maier, R., Mammarella, I., Manca, G., Marcolla, B., Margolis, H. A., Marras, S., Massman, W., Mastepanov, M., Matamala, R., Matthes, J. H., Mazzenga, F., McCaughey, H., McHugh, I., McMillan, A. M. S., Merbold, L., Meyer, W., Meyers, T., Miller, S. D., Minerbi, S., Moderow, U., Monson, R. K., Montagnani, L., Moore, C. E., Moors, E., Moreaux, V., Moureaux, C., Munger, J. W., Nakai, T., Neirynck, J., Nesic, Z., Nicolini, G., Noormets, A., Northwood, M., Nosetto, M., Nouvellon, Y., Novick, K., Oechel, W., Olesen, J. E., Ourcival, J.-M., Papuga, S. A., Parmentier, F.-J., Paul-Limoges, E., Pavelka, M., Peichl, M., Pendall, E., Phillips, R. P., Pilegaard, K., Pirk, N., Posse, G., Powell, T., Prasse, H., Prober, S. M., Rambal, S., Rannik, Ü., Raz-Yaseef, N., Rebmann, C., Reed, D., Dios, V. R. de, Restrepo-Coupe, N., Reverter, B. R., Roland, M., Sabbatini, S., Sachs, T., Saleska, S. R., Sánchez-Cañete, E. P., Sanchez-Mejia, Z. M., Schmid, H. P., Schmidt, M., Schneider, K., Schrader, F., Schroder, I., Scott, R. L., Sedlák, P., Serrano-Ortíz, P., Shao, C., Shi, P., Shironya, I., Siebicke, L., Šigut, L., Silberstein, R., Sirca, C., Spano, D., Steinbrecher, R., Stevens, R. M., Sturtevant, C., Suyker, A., Tagesson, T., Takanashi, S., Tang, Y., Tapper, N., Thom, J., Tomassucci, M., Tuovinen, J.-P., Urbanski, S., Valentini, R., van der Molen, M., van Gorsel, E., van Huissteden, K., Varlagin, A., Verfaillie, J., Vesala, T., Vincke, C., Vitale, D., Vygodskaya, N., Walker, J. P., Walter-Shea, E., Wang, H., Weber, R., Westermann, S., Wille, C., Wofsy, S., Wohlfahrt, G., Wolf, S., Woodgate, W., Li, Y., Zampedri, R., Zhang, J., Zhou, G., Zona, D., Agarwal, D., Biraud, S., Torn, M., and Papale, D.: The FLUXNET2015 dataset and the ONEFlux processing pipeline for eddy covariance data, Sci. Data, 7, 225, https://doi.org/10.1038/s41597-020-0534-3, 2020.

Pique, G., Fieuzal, R., Al Bitar, A., Veloso, A., Tallec, T., Brut, A., Ferlicoq, M., Zawilski, B.,

1028 Dejoux, J.-F., and Gibrin, H.: Estimation of daily CO2 fluxes and of the components of
1029 the carbon budget for winter wheat by the assimilation of Sentinel 2-like remote sensing
1030 data into a crop model, Geoderma, 376, 114428, 2020.
1031 Reichstein, M., Falge, E., Baldocchi, D., Papale, D., Aubinet, M., Berbigier, P., Bernhofer, C.,
1032 Buchmann, N., Gilmanov, T., Granier, A., Grünwald, T., Havránková, K., Ilvesniemi,
1033 H., Janous, D., Knohl, A., Laurila, T., Lohila, A., Loustau, D., Matteucci, G., Meyers,
1034 T., Miglietta, F., Ourcival, J.-M., Pumpanen, J., Rambal, S., Rotenberg, E., Sanz, M.,
1035 Tenhunen, J., Seufert, G., Vaccari, F., Vesala, T., Yakir, D., and Valentini, R.: On the
1036 separation of net ecosystem exchange into assimilation and ecosystem respiration:
1037 review and improved algorithm, Glob. Chang. Biol., 11, 1424–1439,
1038 https://doi.org/https://doi.org/10.1111/j.1365-2486.2005.001002.x, 2005.
1039 Rivalland, V., Calvet, J.-C., Berbigier, P., Brunet, Y., and Granier, A.: Transpiration and CO 2
1040 fluxes of a pine forest: modelling the undergrowth effect, in: Annales Geophysicae,
1041 291–304, 2005.
1042 Roujean, J.: A tractable physical model of shortwave radiation interception by vegetative
1043 canopies, J. Geophys. Res. Atmos., 101, 9523–9532, 1996.
1044 Scott, R. L., Johnston, M. R., Knowles, J. F., MacBean, N., Mahmud, K., Roby, M. C., and
1045 Dannenberg, M. P.: Interannual variability of spring and summer monsoon growing
1046 season carbon exchange at a semiarid savanna over nearly two decades, Agric. For.
1047 Meteorol., 339, https://doi.org/10.1016/j.agrformet.2023.109584, 2023.
1048 Seneviratne, S. I., Corti, T., Davin, E. L., Hirschi, M., Jaeger, E. B., Lehner, I., Orlowsky, B.,
1049 and Teuling, A. J.: Investigating soil moisture–climate interactions in a changing
1050 climate: A review, Earth-Science Rev., 99, 125–161, 2010.
1051 Sharma, B. R., Gulati, Mohan, Gayathri, Manchanda, S., Ray, I., and Amarasinghe, U.: Water
1052 Productivity Mapping of Major Indian Crops, NABARD and ICRIER, 4, 88–100, 2018.

1053 Tanumihardjo, S. A., McCulley, L., Roh, R., Lopez-Ridaura, S., Palacios-Rojas, N., and
1054 Gunaratna, N. S.: Maize agro-food systems to ensure food and nutrition security in
1055 reference to the Sustainable Development Goals, Glob. Food Sec., 25, 100327,
1056 https://doi.org/10.1016/j.gfs.2019.100327, 2020.
1057 Tardieu, F., Simonneau, T., and Parent, B.: Modelling the coordination of the controls of
1058 stomatal aperture, transpiration, leaf growth, and abscisic acid: update and extension of
1059 the Tardieu–Davies model, J. Exp. Bot., 66, 2227–2237, 2015.
1060 Vadez, V., Pilloni, R., Grondin, A., Hajjarpoor, A., Belhouchette, H., Brouziyne, Y.,
1061 Chehbouni, G., Kharrou, M. H., Zitouna-Chebbi, R., and Mekki, I.: Water use
1062 efficiency across scales: from genes to landscapes, J. Exp. Bot., 74, 4770–4788, 2023.
1063 Yang, L., Qu, H., Zhang, Y., and Li, F.: Effects of partial root-zone irrigation on physiology,
1064 fruit yield and quality and water use efficiency of tomato under different calcium levels,
1065 Agric. Water Manag., 104, 89–94, https://doi.org/10.1016/j.agwat.2011.12.001, 2012.
1066 Yu, G., Song, X., Wang, Q., Liu, Y., Guan, D., Yan, J., Sun, X., Zhang, L., and Wen, X.:
1067 Water-use efficiency of forest ecosystems in eastern China and its relations to climatic
1068 variables, New Phytol., 177, 927–937, https://doi.org/10.1111/j.1469-
1069 8137.2007.02316.x, 2008.
1070 Zhou, S., Yu, B., Huang, Y., and Wang, G.: The effect of vapor pressure deficit on water use
1071 efficiency at the subdaily time scale, Geophys. Res. Lett., 41, 5005 – 5013,
1072 https://doi.org/10.1002/2014GL060741, 2014.
1073